Melrakkaslétta, NE-Iceland:
Volcanic lineaments and petrology

Sigurlaug María Hreinsdóttir

Faculty of Earth Science
University of Iceland
2014

Melrakkaslétta, NE-Iceland: Volcanic lineaments and petrology

Sigurlaug María Hreinsdóttir

60 ECTS thesis submitted in partial fulfillment of a
Magister Scientiarum degree in Geology

Advisors
Karl Grönvold
Haukur Jóhannesson

Faculty Representative
Kristján Jónasson

Faculty of Earth Science
School of Engineering and Natural Sciences
University of Iceland
Reykjavik, May 2014

Melrakkaslétta, NE-Iceland: Volcanic lineaments and petrology

60 ECTS thesis submitted in partial fulfillment of a *Magister Scientiarum* degree in Geology

Faculty of Earth Science
School of Engineering and Natural Sciences
University of Iceland
Askja, Sturlugötu 7
107, Reykjavik
Iceland

Telephone: 525 4000

Bibliographic information:
Sigurlaug María Hreinsdóttir, 2014,
Melrakkaslétta, NE-Iceland: Volcanic lineaments and petrology,
Master's thesis, Faculty of Earth Science, University of Iceland, pp. 50.

Printing: Pixel prentþjónusta ehf.
Reykjavík, Iceland, May 2014

Abstract

Mineralogical and geochemical analysis of 67 basalt samples from Melrakkaslétta reveals three rock types: a) Tholeiitic basalts in the early Quaternary volcanic lineaments along the east coast of the peninsula and the dolerite lava fields covering the central peninsula. b) Evolved high phosphorus basalts with strong Fe-Ti affinities occurring locally in the SE-part and c) olivine tholeiites along the west coast. The tholeiites contain occasional large xenocrysts of bytownite in plagioclase-clinopyroxene groundmass with abundant Fe-Ti oxides. The olivine tholeiite contains large phenocrysts of olivine dispersed in a groundmass of olivine, plagioclase, late clinopyroxene and Fe-Ti oxides.

Formation of Melrakkaslétta during the earliest Quaternary followed a northwards rift-propagation of an inland volcanic lineament with a N fracture orientation (160-59°) (Hjartardóttir, Einarsson, Magnúsdóttir, Björnsdóttir, & Brandsdóttir, 2014) that defines the present SE-coast of the peninsula. During the Quaternary, younger parallel volcanic lineaments formed on the rift side (west) of earlier lineaments. The Fjallgarðar lineament reaches as far north as the Afrétt while at least one younger lineament, now mostly covered by dolerite lavas, probably reached as far north as Hraunhafnartangi.

Blikalónsdalur, a recent graben along the central peninsula, is parallel to the earlier tectonic lineaments. A productive volcanic lineament formed during the last glaciation along the west coast of the peninsula. This lineament is characterized by olivine tholeiites matching the composition of the off-shore volcanism. This youngest volcanic lineament with a NNW fracture orientation (110-159°) (Hjartardóttir, Einarsson, Magnúsdóttir, Björnsdóttir, & Brandsdóttir, 2014) is subparallel to all other volcanic structures of the peninsula and its south-termination is connected to the junction of the rift-zone and the GOR that runs into Melrakkaslétta in Núpasveit.

Ágrip

Safnað var 67 bergsýnum á Melrakkasléttu til greiningar á textúr og efnasamsetningu bergs og steinda. Þrjár berggerðir eru á Melrakkasléttu: a) þóleiítbasalt, ríkjandi í myndununum austast og í grágrýtisfláka mið-sléttunnnar. b) Þróað fosfór-ríkt basalt, sem líkist Fe-Ti basalti, kemur fyrir staðbundið við elstu myndanirnar suðaustast á Melrakkasléttu og c) ólivínþóleiít á vesturströnd Melrakkasléttu. Þóleiítið er með stóra bytownít framanddíla í Fe-Ti oxíð ríkum grunnmassa. Ólivínþóleiítið er með stóra ólivíndíla í ólívín og plagíóklas grunnmassa þar sem klínópýroxen og Fe-Ti oxíð myndast undir lokin.

Myndun Melrakkasléttu hófst í upphafi kvarter tímabilsins með framrás sprungusveims til norðurs þar sem stefna sprungna er í N (á bilinu 160-59°) (Hjartardóttir, Einarsson, Magnúsdóttir, Björnsdóttir, & Brandsdóttir, 2014), þar sem nú er suðaustur strönd Melrakkasléttu. Á kvarter tímabilinu mynduðust yngri samsíða sprungusveimar rekmegin (vestan) við eldri sprungusveimana. Fjallgarðasveimurinn nær norður að Afrétt en að minnsta kosti einn yngri sprungusveimur, sem nú er að mestu hulinn grágrýtishrauni, nær að líkindum norður undir Hraunhafnartanga.

Blikalónsdalur, ung sigdæld um miðja Melrakkasléttu, er samsíða eldri myndunum. Sprungusveimur með mikilli gosvirkni frá síðasta jökulskeiði myndar vesturströnd Melrakkasléttu. Þessi sprungusveimur einkennist af ólivínþóleiíti, áþekku bergi af hafsbotni norðan og vestan við Melrakkasléttu. Þessi yngsti sprungusveimur þar sem stefna sprungna er í NNV (á bilinu 110-159°) (Hjartardóttir, Einarsson, Magnúsdóttir, Björnsdóttir, & Brandsdóttir, 2014) er hliðraður miðað við aðra sprungusveima Melrakkasléttu en suðurendi hans tengist mótum gliðnunarbeltisins og Grímseyjargosbeltisins (GOR), sem gengur inn í Melrakkasléttu í Núpasveit.

Table of Contents

List of Figures

List of Tables

Abbreviations

BSE = Back Scattered Electrons

EDS = Energy Dispersive Spectroscopy

GOR = Grímsey Oblique Ridge

HFSE = High Field Strenght Elements

ICP-AES = Inductively coupled plasma atomic emission spectroscopy

LILE = Large Ion Lithophilic Elements

NRZ = Northern Rift Zone

SEM = Hitachi TM 3000 Tabletop Microscope

Acknowledgements

Níels Óskarsson for good advice and for all the help.

Karl Grönvold and Haukur Jóhannesson for the field trips.

Halldór G. Pétursson for sharing all his data on Melrakkaslétta.

Kári Sævarsson and Orri Kárason for assistance in the field.

Arna Auður Antonsdóttir and Hreinn Pálsson.

The office partners, especially Helga Hilmarsdóttir for lifting my spirit.

Jón Eiríksson for lending me equipment.

Snævarr Guðmundsson for assistance with processing data and for lending me a great hand lens.

Gunnur Gunnarsdóttir and Steingrímur Björnsson in Vellir for great hospitality.

Bói (Guðmundur Örn Benediktsson) in Kópasker for a roof over the head, information and a luxury oatmeal.

Þyrí S. Björgvinsdóttir and Högni Felixson in Krossavík for a roof over the head.

Steinþór Hálfdánarson for a roof over the head in Bjarmaland.

1 Introduction

Melrakkaslétta in the northeast of Iceland defines the termination of the Northern Rift Zone (NRZ) of Iceland. The NRZ consists of a number of subparallel elongated volcanic lineaments, each with a variable intensity of tectonic and volcanic activity. In some parts the individual systems can be reasonably mapped, but in other cases they appear to merge and interfere with each other. Some segments are thought to extend for tens to hundreds of kilometers and the northernmost part of the rift zone, Öxarfjörður and Melrakkaslétta are important regions, as they are also connected to the Tjörnes Fracture Zone and the Grímsey Oblique Rift (GOR). The volcanic systems that lie in the NRZ consist of fissure swarms and sometimes a central volcano, (Einarsson & Sæmundsson, 1987), (Thordarson & Larsen, 2007) and references therein). Where a central volcano is present, it is the focal point of eruptive activity and fissure swarms. They are aligned parallel or subparallel to the main regional spreading (Hartley & Thordarson, 2013).

Melrakkaslétta forms the northwards continuation of the Fremri Námar and Askja volcanic systems. However, the volcanic lineaments of Melrakkaslétta are rotated about 30°W relative to the inland volcanic lineaments. The turning point is where the Grímsey Oblique Rift intersects with the Melrakkaslétta Peninsula.

Blikalónsdalur is a recent narrow rift-graben in the middle of the peninsula. Maps and aerial photographs reveal a marked difference between the areas east and west of Blikalónsdalur. In the western part there are numerous visible fractures on the surface, and the area is arid with no lakes and rivulets. In the eastern part few or no fractures are visible on the surface and many lakes are in the area. This possibly reflects the age relation of the Melrakkaslétta peninsula. While the eastern part appears to display a stepwise formation during the early to late Quaternary

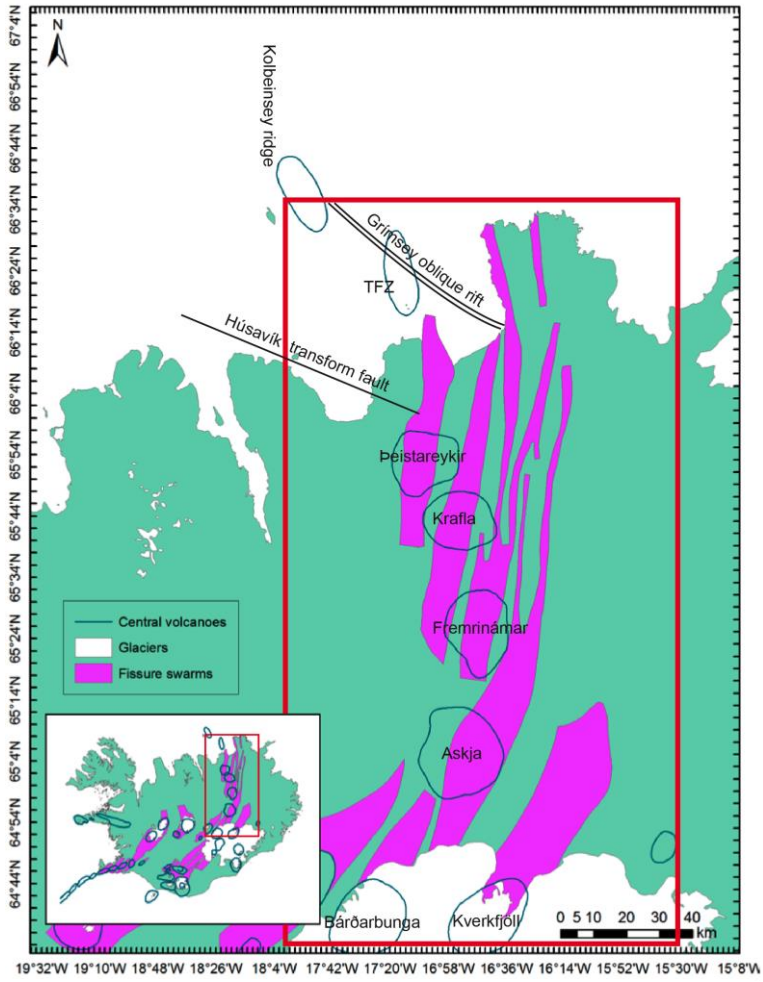

Fig. 1 Melrakkaslétta, Iceland. The Northern Volcanic Zone and its fissure swarms. Red frame in insserted and main Figure shows the location of the Northern Volcanic Zone in Iceland (Einarsson & Sæmundsson, 1987).

the western part is late Quaternary. The working hypothesis of this contribution is that the peninsula is built by a westwards-succession of different volcanic lineaments. The volcanic products of the older easternmost lineaments and their system of eroded hyaloclastite ridges are assumed to have formed impermeable bedrock of the eastern peninsula with its numerous lakes. The eastern lineaments are less volcanically and tectonically active and any old fractures are covered. The western part is younger, more recently active and lies closer to the presently spreading rift-zone. Here, fractures can easily be seen both on aerial photos and in the field. The bedrock is more permeable so the formation of lakes is less common. Blikalónsdalur is a narrow rift valley that divides Melrakkaslétta into the eastern and western part. It is possibly the north termination of a significant rifting event to the south and may be the continuation of craters that formed the Holocene Kerlingarhraun. In some of the volcanic systems in Iceland there is a systematic petrological/geochemical signature that can be used in defining formations and assist in mapping. It is possible that the volcanic units in Melrakkaslétta show such differences. If so, that information could be useful for reconstructing the general formation of Melrakkaslétta and to relate its formation to the more complicated volcano-tectonics in the south or the north of Melrakkaslétta.

The aim of the present research is to look into the geochemistry of Melrakkaslétta and attempt to compare the volcanic lineaments in terms of basalt types and their possible relation to adjoining volcanic lineaments, inland or oceanic.

1.1 Geology

Strictly speaking the name Melrakkaslétta applies to the area that reaches from Snartarstaðarnúpur in the west to Hólsvík, south of Raufarhöfn, in the east. The river Ormarsá is the eastern border, it flows from Axarfjarðarheiði which is the southern border of Melrakkaslétta. But included in the study is the region east of Melrakkaslétta, Fjallgarður and Afrétt. So here the term Melrakkaslétta is used for Melrakkaslétta, Fjallgarður and Afrétt together with Rauðanes and Viðarfjall, south to the old road over Axarfjarðarheiði.

Blikalónsdalur (Fig. 2) is a narrow rift valley that lies in a N-S direction in the middle of Melrakkaslétta, it reaches from Blikalónsey in the north of Melrakkaslétta and disappears further south underneath the Kerlingahraun lava. Kerlingahraun is the youngest lava in the area and erupted from Rauðhólar in Axarfjarðarheiði in early Holocene or about 9000 years ago (Pétursson & Larsen, 1992). Blikalónsdalur divides Melrakkaslétta into E- and W-Melrakkaslétta. In W-Melrakkaslétta Leirhafnarfjöll form a hyaloclastite ridge system on and near the western coast. Fjallgarður in E-Melrakkaslétta is also mostly a hyaloclastite ridge no higher than 457 m at Óttarshnjúkur (Hansen, 2010). The two ridges have a similar direction like Blikalónsdalur and between the two, Melrakkaslétta is mostly flat, covered with tholeiitic basalts. Afrétt, between Fjallgarður and the east coast is older and ranges in age back to Tertiary with formations of both interglacial lavas and hyaloclastites.

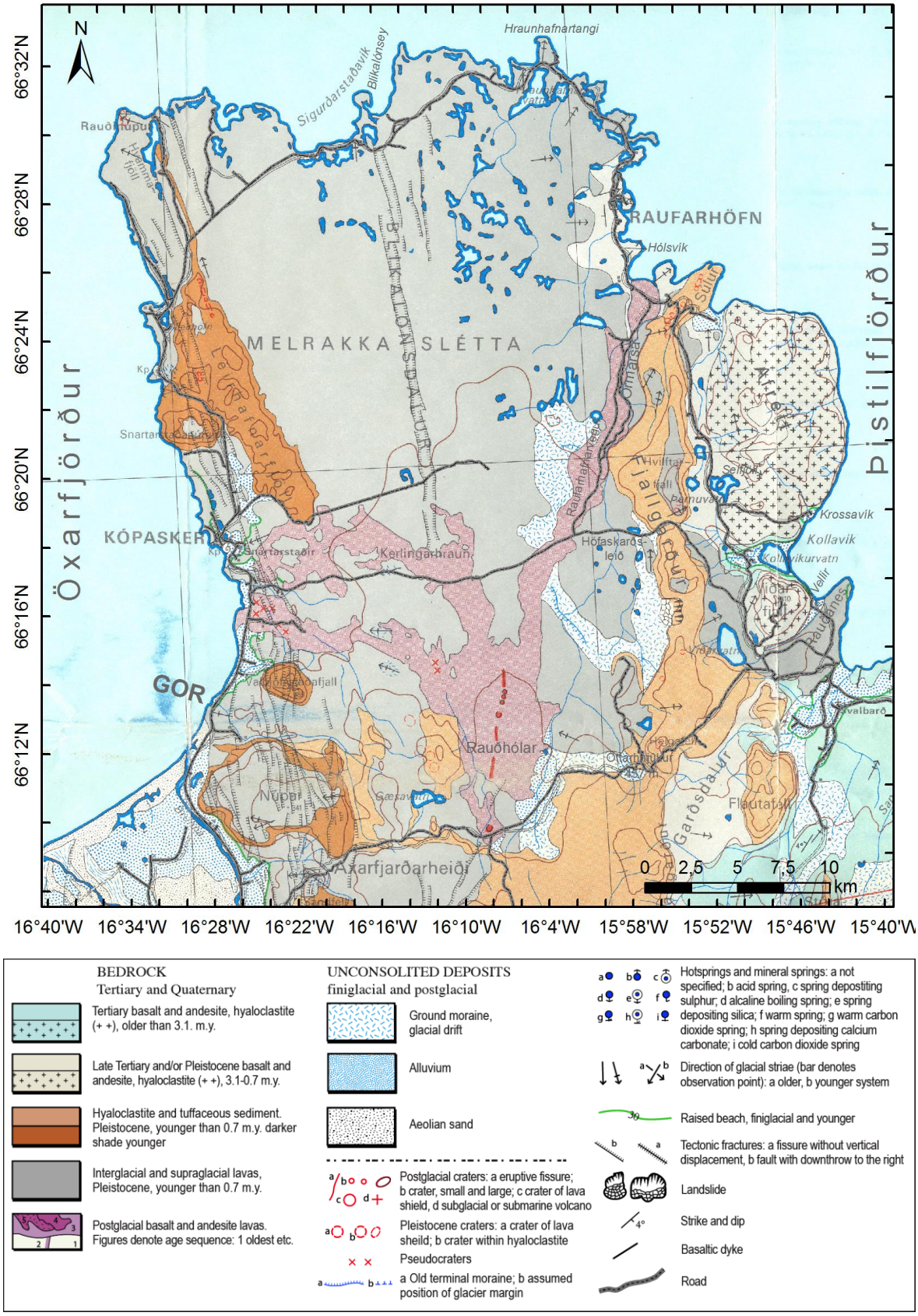

BEDROCK
Tertiary and Quaternary

- Tertiary basalt and andesite, hyaloclastite (+ +), older than 3.1. m.y.
- Late Tertiary and/or Pleistocene basalt and andesite, hyaloclastite (+ +), 3.1-0.7 m.y.
- Hyaloclastite and tuffaceous sediment. Pleistocene, younger than 0.7 m.y. darker shade younger
- Interglacial and supraglacial lavas, Pleistocene, younger than 0.7 m.y.
- Postglacial basalt and andesite lavas. Figures denote age sequence: 1 oldest etc.

UNCONSOLITED DEPOSITS
finiglacial and postglacial

- Ground moraine, glacial drift
- Alluvium
- Aeolian sand
- Postglacial craters: a eruptive fissure; b crater, small and large; c crater of lava shield, d subglacial or submarine volcano
- Pleistocene craters: a crater of lava sheild; b crater within hyaloclastite
- Pseudocraters
- a Old terminal moraine; b assumed position of glacier margin

- Hotsprings and mineral springs: a not specified; b acid spring, c spring depositing sulphur; d alcaline boiling spring; e spring depositing silica; f warm spring; g warm carbon dioxide spring; h spring depositing calcium carbonate; i cold carbon dioxide spring
- Direction of glacial striae (bar denotes observation point): a older, b younger system
- Raised beach, finiglacial and younger
- Tectonic fractures: a fissure without vertical displacement, b fault with downthrow to the right
- Landslide
- Strike and dip
- Basaltic dyke
- Road

Fig. 2 Landmarks in Melrakkaslétta. The map is from (Sæmundsson, 1977), a few landmarks have been added and the road system is updated.

Melrakkaslétta divides into two main parts by age, the western part is younger and less eroded while the eastern part is older and more eroded. The eastern part can also be divided into two parts, Fjallgarður and Afrétt. Afrétt is clearly older than Fjallgarður, it does not rise as high above sea level as Fjallgarður and is more eroded. Where Afrétt meets the ocean its cliffs are tall and steep, such cliffs cannot be found around Melrakkaslétta except for where Snartarstaðarnúpur meets the ocean in Öxarfjörður north of Kópasker.

The ages of the Melrakkaslétta volcanic formations are variable and range from a Holocene lava flow (Kerlingarhraun), down into a Tertiary bedrock in the east. The bedrock in Melrakkaslétta is mostly basalt (Icel. grágrýti) and hyaloclastite (Pétursson H. G., 1997).

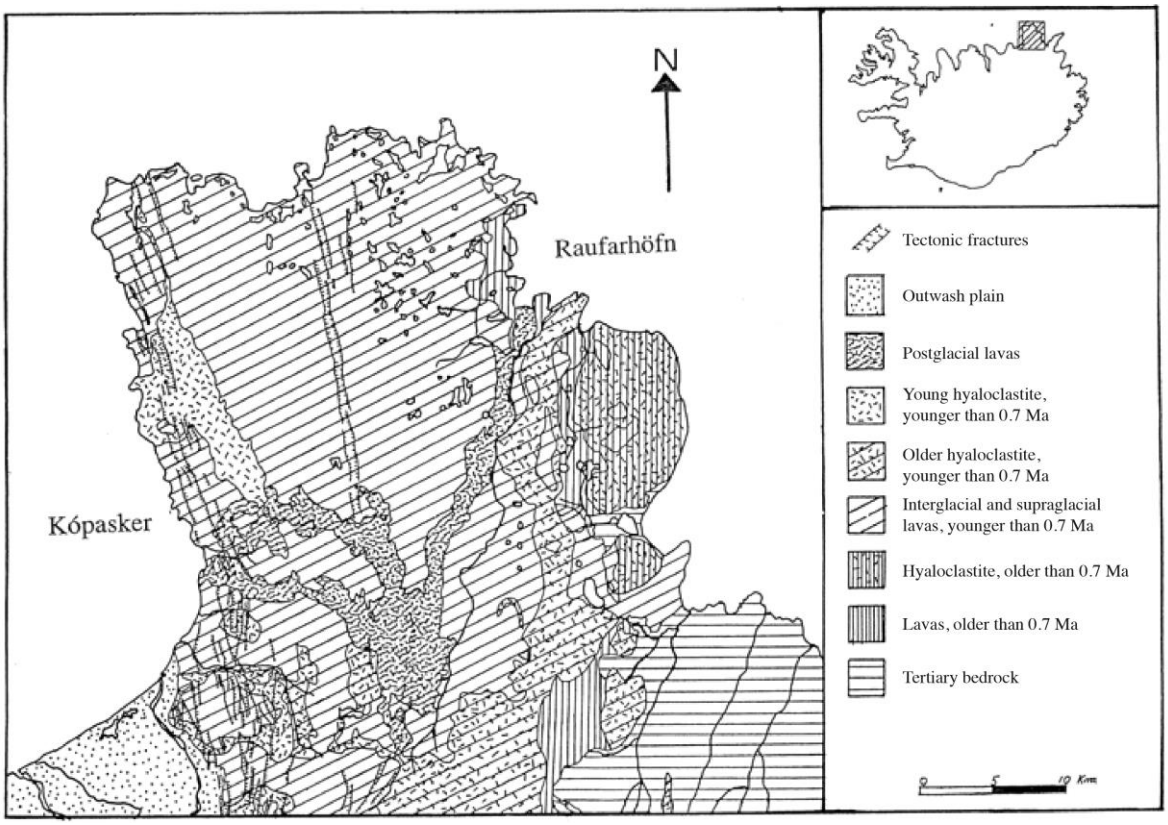

Fig. 3 A bedrock map of Melrakkaslétta (Pétursson H. G., 1997).

The Brunhes-Matuyama palaeomagnetic boundary is said to lie either by Blikalónsdalur and Rauðhólar in the middle of Melrakkaslétta or east of Fjallgarður in Melrakkaslétta. The magnetism of the bedrock beneath is reverse and above the boundary the magnetism is normal. The bedrock west of the boundary has normal magnetism and is therefore younger than 0.78 million years (Pétursson H. G., 1997).

1.2 Earlier research

Some research has been conducted in Melrakkaslétta, the most relevant researchers to this thesis will be mentioned here.

Halldór G. Pétursson did his 4th year assignment (Pétursson H. G., 1979) at the University of Iceland and his Cand. Real. (Pétursson H. G., 1986) at the University of Tromsö. Halldór, later did research for the town of Kópasker (Pétursson H. G., 1997) and did research with Hreggviður Norðdahl and others for reports that the Icelandic Institute of Natural History did for the Icelandic Road Administration previous to building the roads Hófaskarðsleið and Raufarhafnarvegur in Melrakkaslétta e.g. (Pétursson & Norðdahl, 1998), (Albertsson, et al., 2003).

The Icelandic Institute of Natural History published a geological map of NE Iceland in 1977 by Kristján Sæmundsson (Sæmundsson, 1977) and two geological maps; A bedrock geology map and a tectonic map (Jóhannesson & Sæmundsson, 2009) (Jóhannesson & Sæmundsson, 2009).

The first chemical analysis of the Melrakkaslétta basalts appeared in Sigvaldason (1969) where the primitive olivine-tholeiite composition of the youngest subglacial formation on the western margin of Melrakkaslétta (Leirhafnarfjöll) was confirmed as well as the tholeiitic character of Blikalónsdalur and the more recent Kerlingarhraun.

Dieter F. Mertz and others studied dredged pillow-basalt from the area north and northwest of Melrakkaslétta and samples from the Kolbeinsey rift zone during two research cruises with the Polarstern and Poseidon in 1988 and 1989. That research (Mertz, Devey, Todt, Stoffers, & Hofmann, 1991) is mostly focused on trace elements and isotope ratios that suggest that the off-shore volcanism is fed by mantle sources akin to the mantle sources for the Kolbeinsey ridge.

Jóhann Helgason worked for the Icelandic Energy Authority on the petrology of Möðrudalur/Fjallgardar south of Melrakkaslétta and a few reports can be found on that subject, e.g. (Helgason, 1987). In an article summarizing this work it is suggested that „subsurface lateral flow of magma from the neovolcanic zone is responsible for the recent subaerial volcanism in Melrakkaslétta“ (Helgason, 1989). Few chemical analysis of rocks from Melrakkaslétta are found in Helgason´s (1989) article where it is confirmed that the dolerite plains of Melrakkaslétta are tholeiitic basalts of composition similar to the recent Kerlingahraun.

Ásta Rut Hjartardóttir, Páll Einarsson and others (Hjartardóttir, Einarsson, Magnúsdóttir, Björnsdóttir, & Brandsdóttir, 2014) found that transform tectonics of the GOR are found on land in SW-Melrakkaslétta where the volcano-tectonic alignment of the western margin of Melrakkaslétta changes form the earlier N fracture orientation (160-59°) to a NNW fracture orientation (110-159°).

Several chemical analyses of rocks from Melrakkaslétta and the adjoining volcanic systems are found in the petrochemical database at the Institute of Earth Science at the University of Iceland.

2 Sampling and analytical techniques

2.1 Sampling

The fieldwork was conducted during three summers, from 2010-2012. Rock samples were collected at various locations in Melrakkaslétta (Fig. 11) with emphasis on coverage of the different subglacial and interglacial eruption units. Most effort was exercised in finding fresh samples for rock analysis from the Quaternary/Tertiary boundary in the SE-Melrakkaslétta, as well as searching for fresh pillow fragments for analysis of the older subglacial ridges along the east coast of the peninsula, Fjallgarður and also in the older area, Afrétt, east of Fjallgarður. Subglacial rocks along the west coast of Melrakkaslétta (Leirhafnarfjöll) and postglacial rocks across the peninsula were also collected in detail while less effort was made to collect the monotonous badly exposed dolerite field in mid-Melrakkaslétta. Although this thesis focuses on these three subglacial volcanic lineaments of Melrakkaslétta, some samples were taken in Kerlingarhraun and the area south of Leirhafnarfjöll and one in Blikalónsdalur.

Samples were taken as fresh as possible, usually a big rock (5-10 kg) was broken out of a cliff and then broken apart with a sledgehammer, and the fresh core of that rock was taken as a sample. In some locations it was hard to find fresh rocks for sampling, but the samples used for ICP-AES chemical analyzing and the Hitachi TM 3000 Tabletop Microscope (SEM), were chosen with special care.

A collection of 67 samples was processed for analysis. A list of the samples that where collected is shown in Table 2 and brief descriptions of hand specimens are listed in Appendix I.

2.2 Sample preparation and analytical techniques

2.2.1 Whole rock samples

Samples for whole-rock analysis were prepared in the laboratories at the Institute of Earth Science, University of Iceland as following:

1) Samples were crushed in a Retch BB100 Mangan jaw-crusher into grain size less than about 2 mm and then homogenized.
2) About 10 g of each sample was then powdered to about 100 MESH in a Retsch agate mortar.
3) 100 mg of the samples and 200 mg of lithiummetaborate (SPECTROFLUX® $LiBO_2$, melting point 851°C) specpure flux were weighted into a 15 ml carbon crucible and mixed well. Three standards, ATHO, BTH (USGS-BIR-1) and BALK were processed similarly using 250 mg of standard powder and 500 mg of flux.

4) Carbon crucibles were ignited in a Lindberg/Blue oven at 1000°C for 30 minutes and then rapidly cooled to room temperature allowing formation of glass beads from the melt.
5) The glass beads were dissolved in PVC bottles that contained 30 ml of acid mixture (consisting of 5 Vol% HNO_3, 1.33 Vol% HCl and 1.33 Vol% saturated oxalic acid) and the bottles were immediately put into a tilting rotating sample holder. Up to 25 bottles could be put into the holder at once, where the glass beads where left until completely dissolved.
6) Analytical solutions of samples and standards were adjusted to 1% dissolved solids corresponding to sample dilution of 1/300. Major and several trace elements were analyzed on an ICP-AES simultaneous spectrometer (SPECTRO CIROS).
7) ICP-analysis were run with a drift-monitoring sample and the results were corrected for a slight, mostly insignificant, instrumental drift during the analytical session.

2.2.2 SEM samples

Samples for textural SEM-analysis and mineral EDS-analysis (Energy Dispersive Spectroscopy) on the Hitachi TM 3000 Tabletop Microscope were prepared as following:

1) Samples chosen after the results of the whole rock analyzes were complete, see Table 1.
2) Samples were ground roughly on an 400 GRIT abrasive wheel in order to produce flat surfaces for inspection and selection in stereomicroscope.
3) Samples where heated in a Lindberg/Blue oven for 40 minutes at 110°C to vaporize water on their surface.
4) The selected even surface of the samples was glued to round microscope slides (diameter = 1") and cured at 60°C for a few hours.
5) Samples were trimmed on an abrasive wheel to thickness of about 1 mm. Then the samples were polished with abrasive paper on a flat surface (Grit: 400, 800, 1000, 2000).
6) Final polishing of the SEM-samples was made with a water based Buehler Metadi® Supreme Polychrystalline Diamond Suspension (No.40-6632) in a Buehler Minimet 1000 Grinder Polisher at speed 35 and force 6 for 45 minutes.
7) The polished sections were carbon coated in a Cressington Carbon Coater, 208 Carbon with thickness of 6.1 according to the Cressington Thickness Monitor (200-250Å).
8) Running conditions of the Hitachi TM3000 were 15 kV in high vacuum. Textural studies were made at different magnifications of BSE (Back Scattered Electrons) images.
9) EDS-mineral analysis were made on the Hithaci TM3000 at 15 kV under control of the Bruker ESPIRIT® software. Analysis of unknowns and various microprobe standards were made in "Precision Mode" where 250.000 counts are collected for each analyzed point.

Sample
MS7-34
MS8-35
MS26-61
MS30-66
MS31-70
MS38-78
MS40-81
MS61-113

Table 1. SEM samples.

3 Analytical results

3.1 Textural relations

Textural features of tholeiitic lavas are well known, ophitic to subophitic textures dominate olivine tholeiites while evolved tholeiites more frequently show subophitic to cumulative textures. Porphyritic textures are common in olivine tholeiites but the coarse groundmass shows subophitic textures. Textural relations of pillow basalts are varied between porphyritic and cumulative types and are accordingly difficult to interpret. In the following the textural relations of the Melrakkaslétta rocks are described for lavas only.

Three main petrographic groups can be resolved among the Melrakkaslétta rock samples based on SEM-BSE images.

Group 1.

The first group is crystallized with typical olivine tholeiite texture, subophitic with abundant large olivine and plagioclase crystals. Some of the samples are, therefore, with porphyritic texture superimposed on the subophitic coarse groundmass. The large olivine crystals are zoned towards an iron rich rim (Fig. 4) but the anorthite plagioclase megacrysts are unzoned and slightly resorbed on the edges (Fig. 5). The subophitic groundmass is composed of olivine and plagioclase with subordinate amounts of clinopyroxene. Oxide mineralogy of Group 1 texture is characterized by ilmenite and less abundant titanomagnetite. Relations of the ilmenite and the other groundmass minerals are shown in Fig. 6.

It is observed that textural relations of Group 1 conform to long standing cotectic crystallization of olivine and plagioclase in the system An-Di-Fo (Presnall, et al., 1978). As the cotectic composition finally reaches the ol-pl-cpx triple point only subordinate amount of melt is available for the formation of interstitial cpx along with the dominating cotectic phases. Due to the low initial Fe-content of the high-Mg olivine tholeiite melt its FeO content at the triple point is low and the resulting high Ti/Fe-ratio favors the formation of ilmenite along with minor titanomagnetite.

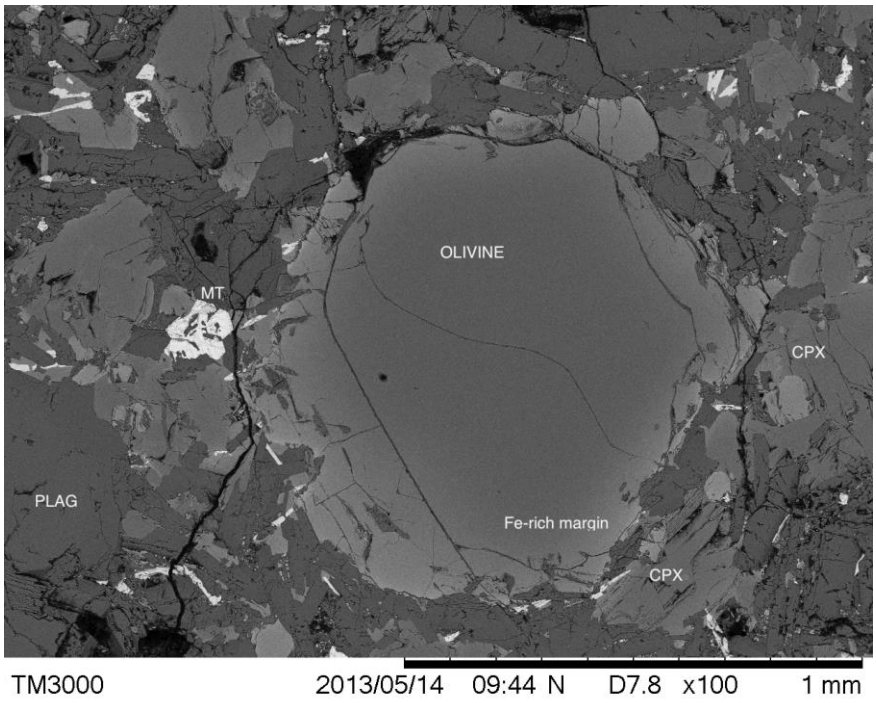

Fig. 4 Sample MS31-70, SEM image. Group 1: Olivine phenocryst zoned towards Fe-rich margins surrounded with groundmass of plagioclase, olivine and clinopyroxene.

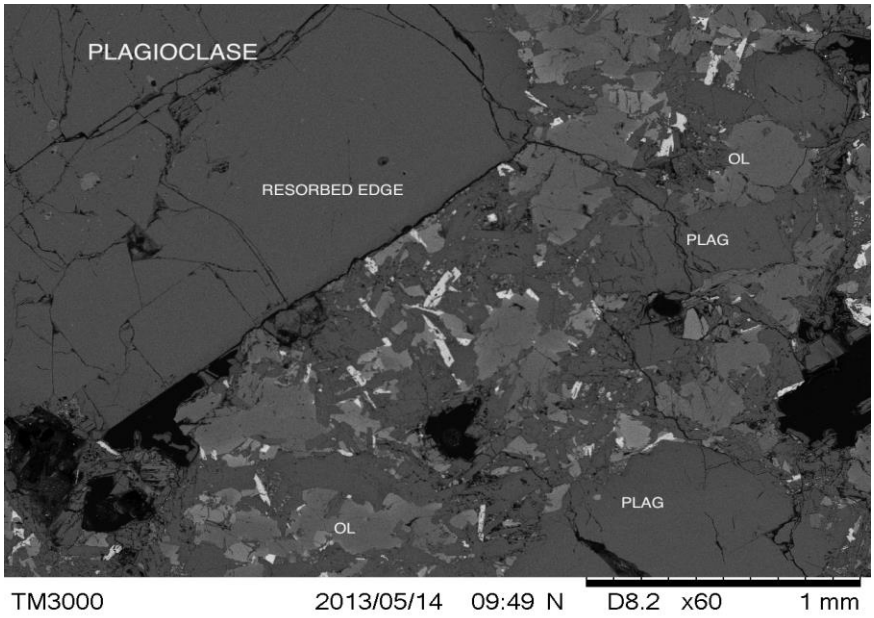

Fig. 5 Sample MS31-70, SEM image. Group 1: Plagioclase megacryst with slightly resorbed edges in contact with fine-grained groundmass.

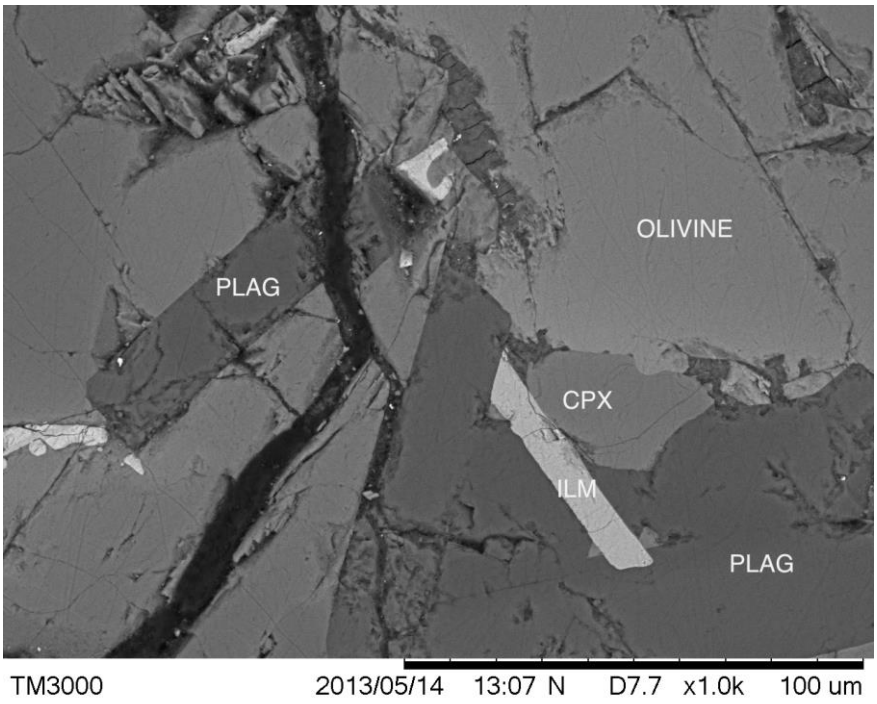

Fig. 6 Sample MS31-70, SEM image. Group 1: Olivine, plagioclase and clinopyroxene in the groundmass join without visible intergranular residual cryptocrystalline mass. Ilmenite appears as euhedral plates or thin sheets in the groundmass.

Group 2

Group 2 textures are characterized by coarse groundmass of plagioclase and clinopyroxene with abundant ilmenite and titanomagnetite. The texture grades from subophitic towards cumulative texture. Occasional phenocrysts (or xenocrysts) of olivine with resorbed rims are found (Fig. 7). The amount of large crystals is too low to classify these rocks as porphyritic. High abundance of the Fe-Ti oxides reflects the increased TiO_2 content of this group which has a strong resemblance with qz-tholeiites although they are surely olivine tholeites with medium to low Mg-contents. This group contains abundant ilmenite and titanomagnetite (Fig. 8). Magnetite has crystallized until the melt reached its solidus as indicated by domains of fine dendritic oxides.

Xenocrysts of gabbroic origin are commonly found in this group (Fig. 9).

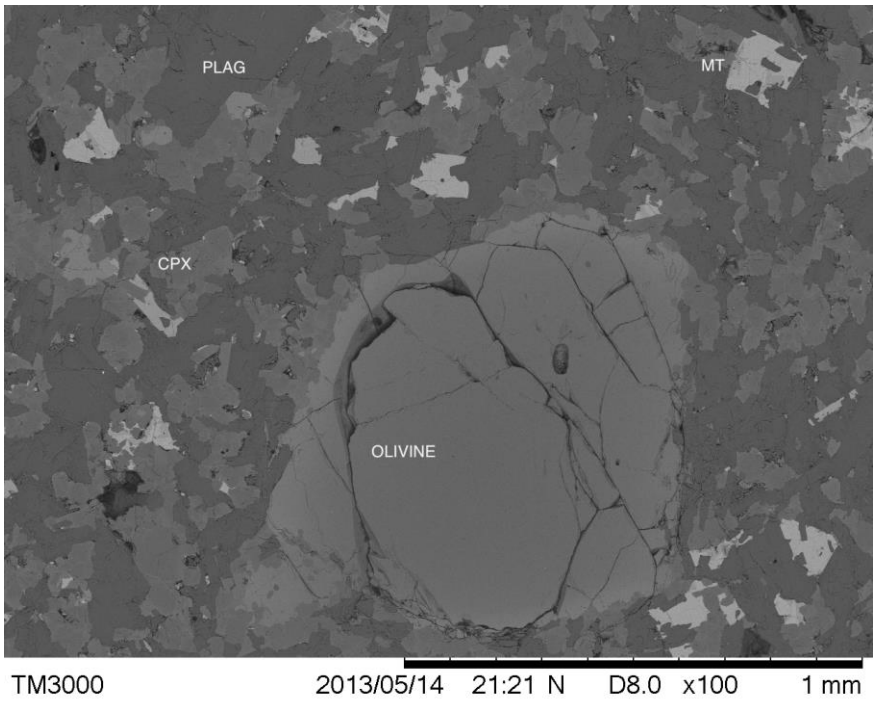

Fig. 7 Sample MS40-81, SEM image. Group 2: Olivine macrocryst with signs of resorbtion enclosed in a coarse plagioclase-clinopyroxene groundmass. Well crystallized Fe-Ti oxides are evenly dispersed throughout the groundmass.

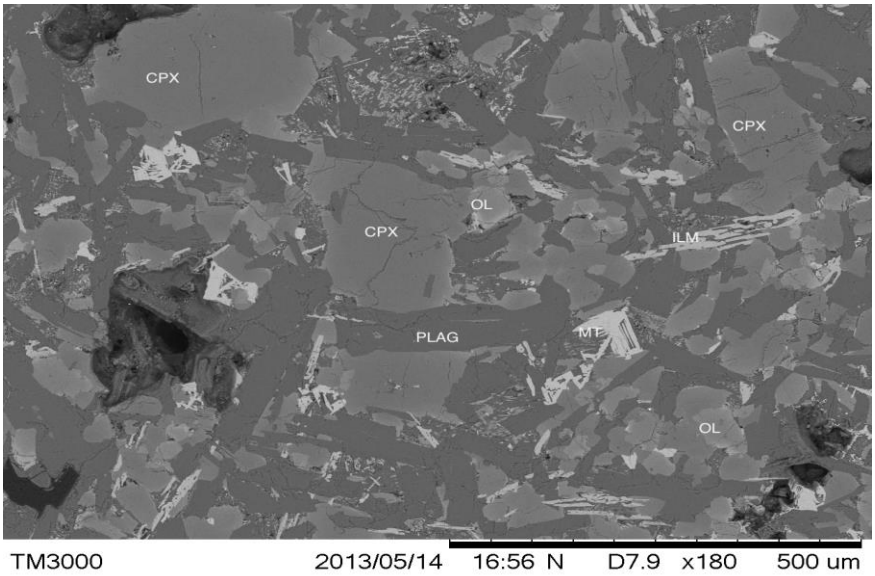

Fig. 8 Sample MS30-66, SEM image. Group 2: Ilmenite blades and dendritic titanomagnetite is evenly dispersed throughout groundmass of plagioclase and clinopyroxene with occational olivine. It is evident that titanomagnetite continued to nucleate until the solidus is reached as shown by domains (upper middle of the Figure) of very small dendritic magnetite.

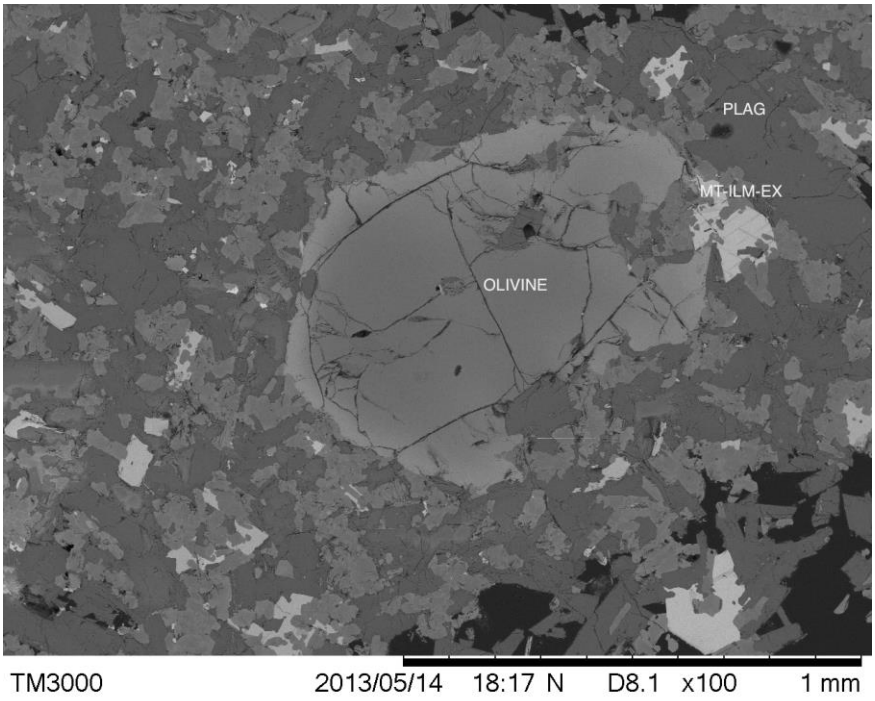

Fig. 9 Sample MS26-61, SEM image. Group 2: Zoned and resorbed xenocryst of olivine in association with titanomagnetite (upper right) with exolution lamellae of ilmenite. This xenocryst assemblage in general and the exolved magnetite in particular is very likely derived from plutonic basalt. Two generations of ilmenite exolution, along both the primary 111 and secondary 100 crystal planes of the magnetite needs time and reflects long-standing oxy-exolution of the primary ulvöspinel (Buddington & Lindsley, 1964). There can be little doubt that these xenocrysts are derived from common gabbro.

Group 3.

Textural group 3 shows sign of high degree of evolution as compared with Groups 1 and 2. Groundmass of plagioclase and clinopyroxene shows slight indications of flow-orientation of plagioclase plates. Fe-Ti oxides are only found on the grain boundaries of the silicates indicating their late crystallization. Large xenocrysts of euhedral plagioclase may indicate assimilation within a crustal magma domain before eruption (Fig.10).

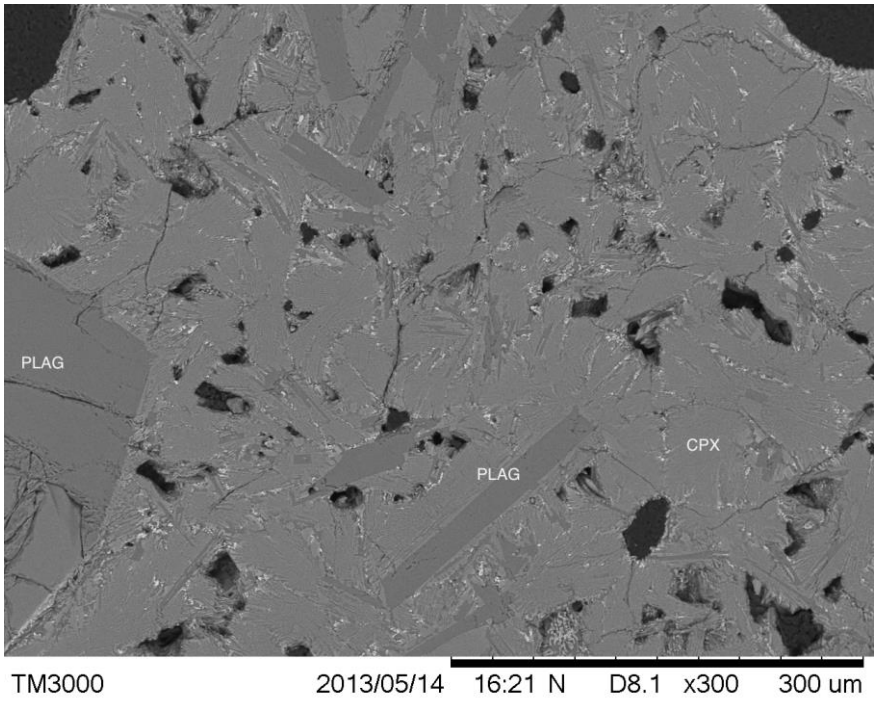

Fig. 10 Sample MS7-34, Group 3: Plagioclase-clinopyroxene groundmass with titanomagnetite and ilmenite on grain boundaries. Occasional euhedral megacrysts (large xenocryst of plagioclase is seen in the lower left of the Figure) of plagioclase are found in this group but olivine was not found and is assumed to be subordinate. In general, this group shows clear signs of higher degree of evolution as compared to textural groups 1 and 2.

The above outlined textural groups are differently exposed across the Melrakkaslétta peninsula. Group 1 is confined to the most recent volcanism along the western margin of Melrakkaslétta while Group 3 rocks are confined to limited area around Kollavík on the eastern margin of the area. Group 3 is found within the oldest rocks on Melrakkaslétta and ranges in age up to the older hyaloclastites.

Group 2 is overwhelmingly the most common textural rock-type of the Melrakkaslétta peninsula and is found in all hyaloclastite formations and the central lava fields of Melrakkaslétta as well as the postglacial Kerlingarhraun belong to this group.

3.2 Whole rock analyses

Both major and trace elements were measured with ICP-AES at the Institute of Earth Science at the University of Iceland. Table 2 shows the results for the major elements and Table 3 the trace elements. The Tables show that the samples from Melrakkaslétta cover a large part of the entire compositional range of rift-zone tholeiites in Iceland. The compositional range will be outlined in a later section.

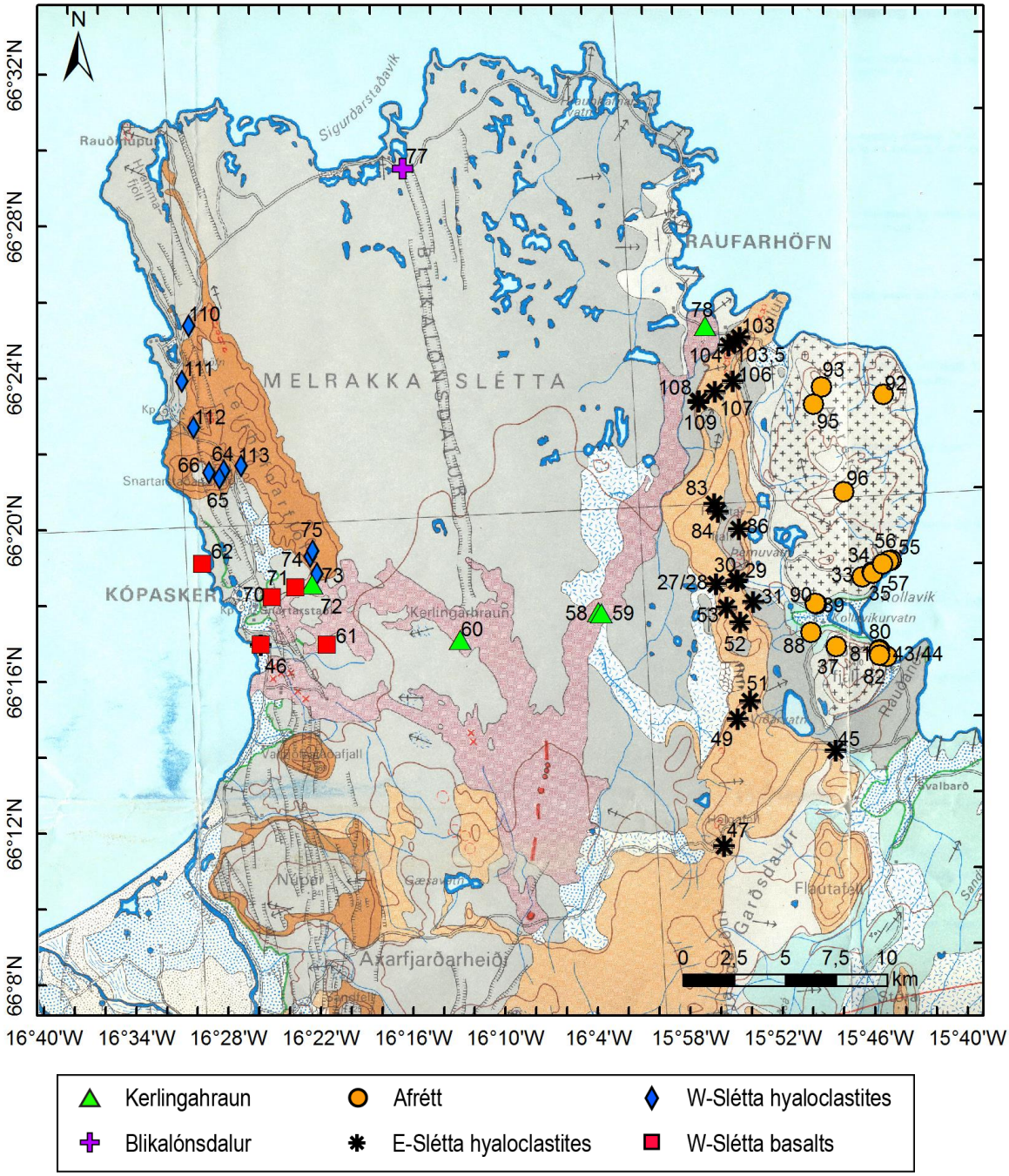

Fig. 11 Location of samples taken in Melrakkaslétta, samples are categorized according to location. The numbers represent the latter number of the sample names, see e.g. Table 2. The map is from (Sæmundsson, 1977), see legend in Fig. 2.

Sample	Lat, N	Long, W	Alt, m	SiO_2	TiO_2	Al_2O_3	Fe_2O_3	MnO	MgO	CaO	Na_2O	K_2O	P_2O_5
MS1m-27	*66,29688*	*-15,91587*	*168*	*49,91*	*2,029*	*13,58*	*12,37*	*0,228*	*7,22*	*11,72*	*2,29*	*0,25*	*0,26*
MS1b-27	66,29688	-15,91587	168	50,35	2,014	13,36	12,28	0,223	6,97	11,82	2,31	0,25	0,28
MS2-28	*66,29688*	*-15,91587*	*168*	*50,50*	*2,042*	*13,39*	*12,61*	*0,221*	*7,50*	*11,18*	*1,93*	*0,24*	*0,26*
MS3-29	66,29800	-15,89181	212	49,74	1,992	13,17	12,48	0,223	7,47	11,99	2,30	0,23	0,26
MS4-30	66,29784	-15,89335	213	50,12	2,258	12,77	13,18	0,234	6,79	11,31	2,47	0,40	0,33
MS5-31	66,28826	-15,87597	173	50,19	2,243	12,84	13,30	0,238	6,62	11,36	2,55	0,25	0,29
MS6-33	66,29707	-15,75608	111	50,01	1,976	13,38	12,06	0,217	7,51	11,92	2,26	0,26	0,27
MS7-34	**66,29896**	**-15,74555**	**76**	**49,45**	**1,669**	**13,46**	**12,65**	**0,226**	**7,26**	**12,44**	**2,31**	**0,18**	**0,22**
MS8-35	**66,29832**	**-15,74440**	**56**	**50,29**	**2,667**	**12,06**	**14,51**	**0,249**	**6,20**	**10,54**	**2,57**	**0,37**	**0,40**
MS9-37	66,26694	-15,78848	340	49,82	2,091	13,49	12,30	0,220	7,28	11,78	2,34	0,25	0,29
MS10-43	66,26155	-15,73395	11	48,82	2,745	13,26	13,60	0,251	6,53	11,36	2,62	0,22	0,44
MS11-44	66,26155	-15,73395	12	49,25	2,057	13,46	12,79	0,226	7,08	11,97	2,45	0,28	0,29
MS12-45	66,22130	-15,79401	200	50,69	2,393	13,15	13,14	0,227	5,96	10,96	2,56	0,41	0,35
MS14-46	66,27900	-16,41500	10	49,88	2,45	13,81	13,15	0,23	6,15	10,99	2,67	0,31	0,23
MS15-47	66,18166	-15,92107	-55	49,32	2,05	14,17	12,40	0,23	6,97	11,86	2,45	0,24	0,19
MS16b-49	66,23701	-15,89902	357	49,78	1,95	14,10	12,09	0,21	7,14	11,73	2,47	0,22	0,17
MS17-51	*66,24480*	*-15,88514*	*300*	*51,07*	*2,07*	*14,39*	*12,53*	*0,22*	*7,13*	*10,15*	*1,76*	*0,39*	*0,17*
MS18-52	*66,27952*	*-15,89145*	*288*	*50,37*	*2,05*	*14,35*	*12,46*	*0,22*	*6,90*	*11,07*	*2,05*	*0,23*	*0,17*
MS19-53	*66,28646*	*-15,90511*	*334*	*50,55*	*2,10*	*14,66*	*12,78*	*0,22*	*6,98*	*10,00*	*2,16*	*0,24*	*0,17*
MS20-55	66,30363	-15,72393	99	49,52	2,15	14,14	12,22	0,22	7,08	11,71	2,37	0,24	0,20
MS21-56	66,30345	-15,72632	106	49,45	2,16	13,99	12,24	0,22	7,30	11,67	2,40	0,24	0,20
MS22-57	66,30221	-15,73323	38	49,24	3,26	13,59	13,38	0,21	6,15	10,76	2,53	0,35	0,37

Table 2. Normalized major elements (Wt%); Explanations of sample names: m = hyaloclastite, b = pillow lava, fínt = small grained, gróft = coarse grained. Lat and long = Decimal degrees. Tuff samples are shown in italic. *Samples used for SEM analyses are shown in* ***bold****. Red samples are High-P basalts, blue samples are evolved tholeiites, black samples are tholeiites and green samples are olivine-tholeiites.*

Sample	Lat, N	Long, W	Alt, m	SiO_2	TiO_2	Al_2O_3	Fe_2O_3	MnO	MgO	CaO	Na_2O	K_2O	P_2O_5
MS23-58	66,28690	-16,04536	148	50,58	1,72	13,71	12,38	0,23	6,81	11,61	2,39	0,24	0,18
MS24-59	66,28640	-16,04219	148	50,08	1,69	13,82	12,37	0,22	6,94	11,96	2,40	0,23	0,16
MS25-60	66,27741	-16,19739	157	50,46	1,60	13,94	11,99	0,22	7,02	11,87	2,40	0,23	0,15
MS26-61	**66,27782**	**-16,34327**	**73**	**49,77**	**2,46**	**13,91**	**13,23**	**0,23**	**5,94**	**11,09**	**2,71**	**0,31**	**0,22**
MS27-62	66,31554	-16,47580	9	49,68	2,45	14,03	13,01	0,23	6,09	11,11	2,71	0,30	0,24
MS28b-64	66,35636	-16,44763	198	49,76	1,84	14,29	12,12	0,22	6,69	12,03	2,54	0,22	0,17
MS28m-64	*66,35636*	*-16,44763*	*198*	*51,32*	*1,87*	*14,53*	*12,18*	*0,22*	*6,80*	*10,14*	*2,24*	*0,43*	*0,14*
MS29-65	*66,35325*	*-16,45300*	*288*	*50,95*	*1,87*	*14,72*	*12,30*	*0,22*	*6,93*	*10,01*	*2,09*	*0,23*	*0,14*
MS30-66	**66,35587**	**-16,46419**	**270**	**50,04**	**1,90**	**14,01**	**12,35**	**0,22**	**6,77**	**11,73**	**2,47**	**0,19**	**0,18**
MS31-70	**66,29971**	**-16,40099**	**52**	**48,87**	**0,79**	**20,11**	**6,63**	**0,12**	**6,59**	**14,81**	**1,81**	**0,10**	**0,07**
MS32-71	66,30353	-16,37489	80	49,86	2,54	13,61	13,54	0,24	6,12	10,85	2,58	0,29	0,24
MS33-72	66,30472	-16,35631	78	50,48	1,75	13,89	12,17	0,23	6,78	11,69	2,45	0,26	0,17
MS34b-73	66,30959	-16,35069	156	49,77	1,09	16,82	8,85	0,16	7,20	13,68	2,09	0,12	0,10
MS34m-73	66,30959	-16,35069	156	50,04	1,09	17,56	8,76	0,16	7,11	12,89	1,97	0,19	0,09
MS35b-74	66,31716	-16,35731	155	49,79	1,07	17,09	8,63	0,16	7,16	13,76	2,02	0,11	0,09
MS35m-74	66,31716	-16,35731	155	49,82	1,15	16,87	9,25	0,17	7,28	13,16	1,93	0,14	0,10
MS36-75	66,31944	-16,35429	185	49,18	1,11	17,14	8,97	0,18	7,14	13,88	2,08	0,12	0,10
MS37-77	66,48580	-16,23772	10	49,88	1,71	14,29	11,50	0,20	7,39	12,17	2,40	0,17	0,15
MS38-78	**66,41041**	**-15,91391**	**16**	**50,39**	**1,71**	**13,83**	**12,25**	**0,23**	**6,91**	**11,73**	**2,40**	**0,25**	**0,17**
MS39-80	66,26449	-15,74152	90	49,68	1,62	13,84	12,09	0,22	7,24	12,51	2,35	0,17	0,14
MS40-81	**66,26397**	**-15,74218**	**115**	**49,60**	**2,02**	**14,86**	**11,62**	**0,20**	**6,76**	**11,90**	**2,49**	**0,22**	**0,18**
MS41b-82	66,26215	-15,74191	134	49,44	2,21	14,08	12,38	0,22	6,98	11,59	2,49	0,26	0,20
MS41m-82	*66,26215*	*-15,74191*	*134*	*50,00*	*2,20*	*14,63*	*12,47*	*0,23*	*7,41*	*9,97*	*2,55*	*0,21*	*0,19*
MS42-83	66,33228	-15,91298	259	49,71	1,98	14,29	11,95	0,22	6,94	11,89	2,48	0,22	0,18

Table 2 (continued).

Sample	Lat, N	Long, W	Alt, m	SiO_2	TiO_2	Al_2O_3	Fe_2O_3	MnO	MgO	CaO	Na_2O	K_2O	P_2O_5
MS43b-84	66,32844	-15,91003	269	49,55	2,03	14,15	12,33	0,24	6,94	11,76	2,44	0,24	0,19
MS43m-84	66,32844	-15,91003	269	49,22	2,07	14,66	12,36	0,23	6,93	11,58	2,38	0,24	0,18
MS45-88	66,27369	-15,81553	97	50,03	2,10	13,62	13,00	0,24	6,32	11,46	2,52	0,30	0,28
MS46-89	66,28604	-15,80762	43	49,79	2,82	13,16	14,01	0,24	6,03	10,55	2,70	0,32	0,24
MS47fínt-90	66,28623	-15,80887	71	49,75	2,07	13,91	12,97	0,23	6,39	11,52	2,51	0,26	0,26
MS47gróft-90	66,28623	-15,80887	71	49,37	1,99	14,36	11,87	0,21	7,43	11,92	2,34	0,19	0,18
MS48-92	*66,37656*	*-15,72340*	*164*	*49,71*	*2,03*	*14,28*	*11,84*	*0,21*	*7,18*	*11,86*	*2,34*	*0,21*	*0,19*
MS49-93	66,38119	-15,79029	171	49,27	2,24	13,98	12,43	0,22	7,09	11,71	2,46	0,24	0,20
MS50-95	*66,37399*	*-15,79985*	*198*	*50,73*	*2,17*	*14,55*	*12,31*	*0,22*	*7,11*	*10,12*	*2,10*	*0,36*	*0,19*
MS51-96	66,33483	-15,77152	301	49,04	2,02	14,52	12,10	0,21	7,42	11,82	2,37	0,13	0,18
MS52-103	*66,40474*	*-15,87634*	*114*	*50,02*	*2,03*	*14,35*	*12,28*	*0,22*	*7,42*	*10,89*	*2,14*	*0,31*	*0,18*
MS52,5-103,5	66,40300	-15,88200	109	49,37	2,01	14,32	12,22	0,22	6,91	11,96	2,44	0,23	0,18
MS53-104	*66,40146*	*-15,88905*	*104*	*50,34*	*2,05*	*14,81*	*12,47*	*0,22*	*7,11*	*10,16*	*2,09*	*0,42*	*0,18*
MS54-106	*66,38570*	*-15,88628*	*175*	*50,66*	*2,01*	*14,40*	*12,14*	*0,21*	*7,18*	*10,72*	*2,01*	*0,30*	*0,22*
MS55-107	66,38145	-15,90679	156	49,33	2,07	14,30	12,27	0,22	6,98	11,75	2,51	0,24	0,20
MS56-108	66,37782	-15,92495	188	49,30	1,87	14,62	11,77	0,21	7,33	12,00	2,40	0,21	0,17
MS57-109	*66,37753*	*-15,92546*	*197*	*50,83*	*1,99*	*14,34*	*12,13*	*0,22*	*7,21*	*10,59*	*2,05*	*0,30*	*0,19*
MS58-110	66,42064	-16,47974	144	49,22	1,09	17,32	8,75	0,16	7,06	14,03	2,04	0,11	0,10
MS59-111	66,39647	-16,48976	57	49,37	1,12	16,91	8,95	0,17	7,34	13,71	2,08	0,13	0,10
MS60-112	66,37580	-16,47907	77	49,79	1,11	16,63	8,96	0,17	7,29	13,61	2,12	0,13	0,10
MS61-113	**66,35836**	**-16,42890**	**80**	**48,92**	**1,13**	**16,86**	**9,42**	**0,17**	**7,47**	**13,63**	**2,07**	**0,12**	**0,10**

Table 2 (continued).

Sample	Lat, N	Long, W	Alt, m	Sc	Cr	Co	Ni	Cu	Zn	Sr	Y	Zr	Ba	La	V
MS1m-27	*66,29688*	*-15,91587*	*168*	*47*	*217*	*63*	*73*	*158*	*55*	*190*	*36*	*120*	*51*	*11*	*350*
MS1b-27	66,29688	-15,91587	168	46	190	62	66	155	54	193	36	119	50	10	361
MS2-28	*66,29688*	*-15,91587*	*168*	*48*	*219*	*63*	*78*	*158*	*54*	*189*	*36*	*121*	*50*	*12*	*332*
MS3-29	66,29800	-15,89181	212	48	212	62	73	155	56	191	35	118	48	11	379
MS4-30	66,29784	-15,89335	213	46	78	73	62	160	57	203	39	140	68	12	401
MS5-31	66,28826	-15,87597	173	46	88	67	57	130	57	185	40	129	54	12	434
MS6-33	66,29707	-15,75608	111	44	241	64	93	149	51	176	36	117	46	10	379
MS7-34	**66,29896**	**-15,74555**	**76**	**47**	**162**	**60**	**71**	**166**	**53**	**161**	**34**	**98**	**37**	**9**	**352**
MS8-35	**66,29832**	**-15,74440**	**56**	**46**	**89**	**69**	**54**	**166**	**66**	**179**	**53**	**170**	**62**	**15**	**454**
MS9-37	66,26694	-15,78848	340	44	216	64	86	163	53	179	38	123	48	10	388
MS10-43	66,26155	-15,73395	11	42	78	71	54	155	62	294	46	179	78	18	414
MS11-44	66,26155	-15,73395	12	46	195	64	66	150	51	197	37	124	53	12	370
MS12-45	66,22130	-15,79401	200	44	58	66	47	203	62	212	42	149	69	14	414
MS14-46	66,27900	-16,41500	10	43	100	62	55	92	71	195	38	150	63	13	416
MS15-47	66,18166	-15,92107	-55	46	194	61	70	193	58	192	33	116	50	13	342
MS16b-49	66,23701	-15,89902	357	46	217	58	69	162	56	191	32	113	47	11	337
MS17-51	*66,24480*	*-15,88514*	*300*	*47*	*193*	*61*	*69*	*185*	*63*	*199*	*34*	*119*	*51*	*12*	*266*
MS18-52	*66,27952*	*-15,89145*	*288*	*47*	*197*	*61*	*63*	*177*	*61*	*198*	*33*	*116*	*50*	*11*	*296*
MS19-53	*66,28646*	*-15,90511*	*334*	*47*	*183*	*62*	*66*	*190*	*61*	*198*	*34*	*120*	*52*	*13*	*292*
MS20-55	66,30363	-15,72393	99	44	205	61	85	153	59	183	36	122	51	12	366
MS21-56	66,30345	-15,72632	106	44	205	62	87	169	59	184	35	122	49	12	365
MS22-57	66,30221	-15,73323	38	40	66	71	57	152	71	289	45	219	103	24	406

Table 3. Normalized trace elements (ppm); Explanations of sample names: m = hyaloclastite, b = pillow lava, fínt = small grained, gróft = coarse grained. Lat and long = Decimal degrees. Tuff samples are shown in italic. *Samples used for SEM analyses are shown in* ***bold****. Red samples are High-P basalts, blue samples are evolved tholeiites, black samples are tholeiites and green samples are olivine-tholeiites.*

Sample	Lat, N	Long, W	Alt, m	Sc	Cr	Co	Ni	Cu	Zn	Sr	Y	Zr	Ba	La	V
MS23-58	66,28690	-16,04536	148	47	70	56	56	184	57	166	32	111	56	11	368
MS24-59	66,28640	-16,04219	148	47	75	59	59	171	57	160	31	95	52	12	372
MS25-60	66,27741	-16,19739	157	47	74	57	58	157	55	160	30	95	52	10	341
MS26-61	**66,27782**	**-16,34327**	**73**	**43**	**101**	**61**	**53**	**79**	**62**	**200**	**38**	**149**	**64**	**14**	**404**
MS27-62	66,31554	-16,47580	9	43	102	62	54	112	64	201	39	153	65	16	405
MS28b-64	66,35636	-16,44763	198	45	118	58	47	130	56	181	31	107	48	10	336
MS28m-64	*66,35636*	*-16,44763*	*198*	*47*	*136*	*60*	*53*	*174*	*58*	*227*	*33*	*117*	*55*	*11*	*266*
MS29-65	*66,35325*	*-16,45300*	*288*	*47*	*131*	*63*	*53*	*167*	*59*	*276*	*32*	*110*	*48*	*13*	*261*
MS30-66	**66,35587**	**-16,46419**	**270**	**46**	**122**	**59**	**47**	**157**	**60**	**179**	**33**	**113**	**49**	**13**	**345**
MS31-70	**66,29971**	**-16,40099**	**52**	**30**	**249**	**36**	**85**	**80**	**34**	**197**	**16**	**46**	**20**	**8**	**179**
MS32-71	66,30353	-16,37489	80	44	101	63	54	85	66	195	38	155	68	15	431
MS33-72	66,30472	-16,35631	78	47	75	58	54	166	56	162	33	105	58	12	374
MS34b-73	66,30959	-16,35069	156	41	239	47	71	133	41	163	21	65	28	9	255
MS34m-73	66,30959	-16,35069	156	41	243	47	74	134	41	211	22	66	31	9	222
MS35b-74	66,31716	-16,35731	155	40	237	44	71	114	41	164	21	64	27	9	249
MS35m-74	66,31716	-16,35731	155	43	255	49	76	136	43	157	23	69	29	9	248
MS36-75	66,31944	-16,35429	185	41	235	46	77	130	41	166	22	66	30	10	260
MS37-77	66,48580	-16,23772	10	46	234	56	83	178	54	172	29	97	40	10	330
MS38-78	**66,41041**	**-15,91391**	**16**	**47**	**67**	**57**	**55**	**192**	**58**	**163**	**32**	**123**	**54**	**12**	**356**
MS39-80	66,26449	-15,74152	90	48	172	56	70	172	53	156	30	89	35	12	357
MS40-81	**66,26397**	**-15,74218**	**115**	**42**	**162**	**56**	**64**	**108**	**57**	**194**	**33**	**120**	**48**	**11**	**354**
MS41b-82	66,26215	-15,74191	134	45	188	60	73	176	59	183	35	125	50	12	393
MS41m-82	*66,26215*	*-15,74191*	*134*	*44*	*185*	*62*	*84*	*180*	*61*	*174*	*36*	*128*	*45*	*13*	*350*
MS42-83	66,33228	-15,91298	259	46	199	58	67	177	54	195	32	113	48	13	342

Table 3 (continued).

Sample	Lat, N	Long, W	Alt, m	Sc	Cr	Co	Ni	Cu	Zn	Sr	Y	Zr	Ba	La	V
MS43b-84	66,32844	-15,91003	269	46	192	61	73	180	58	192	33	116	50	12	356
MS43m-84	66,32844	-15,91003	269	47	198	61	65	181	58	198	33	119	52	12	343
MS45-88	66,27369	-15,81553	97	46	98	60	52	141	62	181	38	134	63	16	379
MS46-89	66,28604	-15,80762	43	45	65	65	46	117	70	182	42	170	67	14	464
MS47fínt-90	66,28623	-15,80887	71	46	95	60	45	156	63	181	39	131	57	14	380
MS47gróft-90	66,28623	-15,80887	71	44	223	58	86	139	56	178	33	114	44	11	358
MS48-92	*66,37656*	*-15,72340*	*164*	*43*	*208*	*56*	*82*	*116*	*57*	*183*	*33*	*116*	*46*	*12*	*359*
MS49-93	66,38119	-15,79029	171	45	187	60	75	188	61	184	36	126	51	14	389
MS50-95	*66,37399*	*-15,79985*	*198*	*45*	*198*	*61*	*78*	*168*	*60*	*231*	*36*	*124*	*55*	*13*	*308*
MS51-96	66,33483	-15,77152	301	44	230	60	90	178	61	183	34	114	43	13	355
MS52-103	*66,40474*	*-15,87634*	*114*	*47*	*207*	*61*	*70*	*173*	*58*	*202*	*33*	*115*	*50*	*13*	*335*
MS52,5-103,5	66,40300	-15,88200	109	46	194	59	61	97	56	192	32	114	48	14	349
MS53-104	*66,40146*	*-15,88905*	*104*	*47*	*208*	*60*	*66*	*182*	*59*	*230*	*34*	*118*	*52*	*14*	*278*
MS54-106	*66,38570*	*-15,88628*	*175*	*46*	*203*	*60*	*68*	*183*	*59*	*196*	*33*	*115*	*48*	*13*	*283*
MS55-107	66,38145	-15,90679	156	46	187	59	65	149	58	192	33	117	51	13	348
MS56-108	66,37782	-15,92495	188	46	216	57	65	148	55	194	31	106	44	12	328
MS57-109	*66,37753*	*-15,92546*	*197*	*46*	*200*	*59*	*64*	*179*	*57*	*187*	*32*	*122*	*52*	*11*	*289*
MS58-110	66,42064	-16,47974	144	41	211	44	65	117	40	169	21	94	28	9	245
MS59-111	66,39647	-16,48976	57	41	234	47	71	114	42	167	22	67	29	9	246
MS60-112	66,37580	-16,47907	77	41	236	47	74	123	41	166	22	65	28	10	264
MS61-113	**66,35836**	**-16,42890**	**80**	**42**	**254**	**50**	**80**	**126**	**43**	**162**	**22**	**65**	**29**	**10**	**253**

Table 3 (continued).

3.3 SEM-EDS analysis

The samples for EDS chemical analysis of minerals where chosen based on whole-rock analyses in order to cover spatial distribution and the compositional range of the basalts. Compositional diversity of the samples was considered based on the #Mg vs. TiO_2 graph in Fig. 12) where the samples selected for mineral analysis are shown in red.

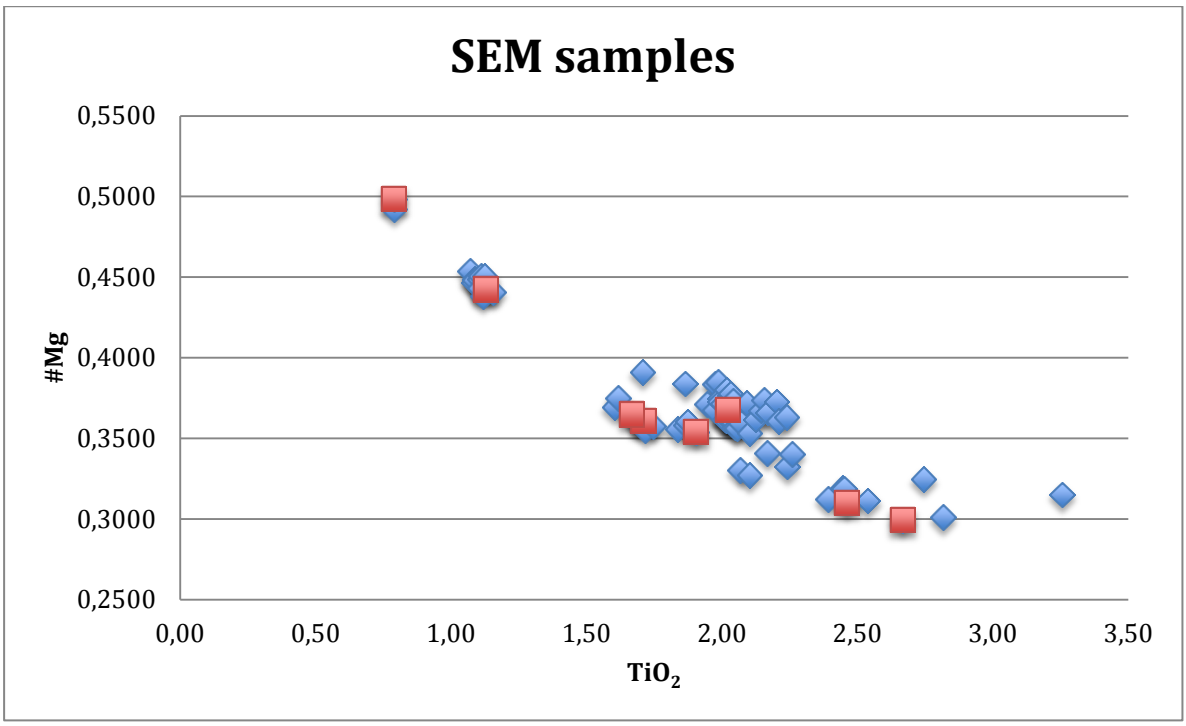

Fig. 12 #Mg vs. TiO_2 showing in red which samples were chosen for SEM analysis.

The EDS analysis tables are ordered by minerals, olivine, plagioclase, clinopyroxene and oxides (Lepage, 2014). See Tables 4-7 here below.

Sample	SiO_2	FeO	MgO	SUM	%fo
MS31-70	38,60	11,62	49,79	100,01	88,4
MS31-70	35,85	33,33	30,48	99,67	62,0
MS31-70	35,90	32,99	30,65	99,54	62,4
MS31-70	36,54	36,56	26,91	100,01	56,8
MS31-70	34,75	40,14	24,75	99,64	52,4
MS31-70	37,28	30,41	31,93	99,62	65,2
MS31-70	34,44	42,17	22,83	99,44	49,1
MS30-66	36,42	32,52	30,59	99,53	62,6
MS30-66	35,49	34,71	29,39	99,59	60,1
MS40-81	37,27	23,11	39,26	99,64	75,2
MS38-78	41,08	26,25	32,12	99,45	68,6
MS38-78	42,08	10,58	47,35	100,01	88,9
MS26-61	36,77	23,95	38,91	99,64	74,3
MS26-61	33,78	50,32	15,05	99,14	34,8

Table 4. Olivine EDS mineral analysis, Wt%.

Sample	SiO_2	Al_2O_3	CaO	Na_2O	SUM	%an
MS31-70	45,73	36,62	16,27	1,44	100,06	86,2
MS31-70	46,07	34,42	18,32	1,22	100,03	89,2
MS31-70	47,53	34,87	13,72	2,66	98,77	74,1
MS31-70	46,65	35,83	15,49	1,59	99,56	84,3
MS31-70	46,91	33,61	18,09	1,46	100,08	87,3
MS61-113	45,00	36,70	14,32	2,65	98,67	74,9
MS61-113	49,05	33,43	13,28	3,13	98,89	70,1
MS61-113	50,44	33,12	12,77	3,26	99,59	68,4
MS7-34	47,46	34,89	14,01	2,38	98,75	76,5
MS7-34	47,81	34,71	14,75	2,25	99,52	78,3
MS7-34	45,45	36,09	15,66	1,68	98,88	83,7
MS7-34	44,86	37,05	14,69	2,17	98,77	78,9
MS7-34	46,04	35,03	16,86	1,20	99,13	88,6
MS7-34	50,18	32,57	12,58	3,46	98,79	66,8
MS30-66	54,10	29,61	12,17	3,07	98,94	68,7
MS30-66	52,32	31,43	10,68	4,15	98,58	58,8
MS40-81	52,78	29,87	13,04	3,04	98,73	70,3
MS40-81	50,28	32,61	12,88	3,11	98,87	69,6
MS8-35	44,50	36,77	16,80	1,04	99,11	89,9
MS8-35	44,38	36,34	17,09	1,19	99,01	88,8
MS8-35	51,03	32,03	11,40	3,91	98,37	61,7
MS8-35	49,34	33,02	12,55	3,88	98,79	64,1
MS38-78	52,32	30,44	12,93	3,04	98,72	70,2
MS38-78	51,92	30,19	13,66	2,81	98,58	72,9
MS38-78	53,14	28,81	12,80	3,25	97,99	68,5
MS26-61	52,99	30,20	12,50	3,07	98,76	69,2

Table 5. Plagioclase EDS mineral analysis, Wt%.

Sample	SiO_2	TiO_2	Al_2O_3	FeO	MnO	MgO	CaO	Na_2O	SUM	% wo	% en	% fs
MS31-70	52,78	0,46	2,79	8,03	0,23	17,30	18,34	0,06	100,00	37,7	49,5	12,9
MS31-70	53,73	0,33	2,70	8,03	0,20	16,08	18,81	0,12	100,00	39,6	47,2	13,2
MS31-70	52,51	0,00	2,87	10,53	0,00	15,67	18,41	0,18	100,17	38,0	45,0	17,0
MS31-70	54,41	0,36	2,33	5,85	0,00	17,26	19,72	0,08	100,01	40,8	49,7	9,5
MS31-70	52,16	0,64	2,54	11,19	0,30	14,54	18,48	0,15	100,00	39,0	42,6	18,4
MS31-70	54,39	0,50	2,49	6,95	0,05	17,83	17,72	0,08	100,00	36,9	51,7	11,3
MS30-66	49,63	1,29	5,10	10,19	0,24	17,91	14,91	0,73	100,00	31,2	52,2	16,6
MS30-66	51,16	0,46	1,46	23,43	0,56	12,26	10,47	0,20	100,00	22,8	37,2	39,9
MS40-81	52,21	0,77	1,74	15,38	0,23	13,34	16,25	0,08	100,00	34,7	39,6	25,6
MS40-81	54,49	0,55	2,68	9,46	0,19	14,92	17,38	0,33	100,00	38,2	45,6	16,2
MS40-81	51,79	0,54	2,28	15,39	0,38	12,83	16,44	0,33	100,00	35,5	38,6	25,9
MS8-35	53,36	0,38	4,14	6,56	0,16	16,78	18,49	0,13	100,00	39,4	49,7	10,9
MS8-35	51,40	0,69	4,81	7,44	0,13	17,53	17,66	0,33	100,00	36,9	51,0	12,1
MS38-78	53,01	0,77	2,79	11,53	0,17	16,35	15,13	0,23	100,00	32,3	48,5	19,2
MS38-78	51,31	1,15	3,18	11,87	0,14	14,93	17,12	0,30	100,00	36,3	44,1	19,6

Table 6. Clinopyroxene EDS mineral analysis, Wt%.

Sample	TiO2	Al_2O_3	FeO	MnO	MgO	SUM	%usp/%mt	%im/%hm	T°C
MS31-70	53,52	0,81	42,74	0,27	2,66	100		99.2/0.8	
MS31-70	53,03	2,84	41,52	0,24	2,38	100		97.6/2.4	
MS31-70	**21,59**	**1,47**	**75,78**	**0,27**	**0,89**	**100**	**58.8/41.2**		**763**
MS31-70	18,19	2,12	78,29	0,38	1,02	100	49.2/50.8		
MS31-70	25,43	2,48	70,78	0,19	1,13	100	69.1/30.9		
MS31-70	28,58	2,20	67,98	0,14	1,11	100	78.0/22.0		
MS31-70	51,16	0,67	46,60	0,25	1,32	100		95.7/4.3	
MS31-70	51,72	0,57	46,09	0,27	1,35	100		96.8/3.2	
MS31-70	26,26	1,68	70,70	0,15	1,22	100	71.6/28.4		
MS30-66	23,48	1,76	74,19	0,29	0,28	100	64.3/35.7		
MS30-66	22,44	1,92	74,88	0,21	0,55	100	61.2/38.8		
MS30-66	23,09	2,06	74,04	0,22	0,59	100	63.0/37.0		
MS40-81	17,51	1,54	79,90	0,24	0,80	100	47.5/52.5		
MS40-81	23,39	1,59	73,50	0,27	1,24	100	63.6/36.4		
MS40-81	20,99	1,32	76,77	0,23	0,69	100	57.2/42.8		
MS40-81	52,30	0,44	45,38	0,31	1,57	100		97.9/2.1	
MS8-35	25,90	1,52	71,28	0,31	0,99	100	70.8/29.2		
MS8-35	22,27	1,18	75,49	0,14	0,92	100	60.7/39.3		
MS8-35	23,68	1,13	73,57	0,36	1,26	100	64.5/35.5		
MS38-78	14,69	1,52	83,07	0,33	0,39	100	39.9/60.1		
MS38-78	50,42	0,45	46,54	0,44	2,15	100		93.7/6.3	
MS26-61	52,00	0,36	46,35	0,28	1,01	100		97.7/3.3	
MS26-61	51,49	0,38	46,45	0,47	1,21	100		96.6/3.4	
MS26-61	24,88	1,02	73,56	0,22	0,33	100	68.6/31.4		
MS26-61	**21,95**	**2,02**	**74,65**	**0,28**	**1,11**	**100**	**59.7/40.3**		**899**
MS26-61	50,29	0,61	47,74	0,36	1,00	100		94.1/5.9	

Table 7. Fe-Ti Oxides EDS mineral analysis, Wt%.

3.4 Notes on mineral analysis.

Compositional range of minerals in the Melrakkaslétta basalts is given in Tables 4-7 where EDS-analysis of olivine, plagioclase, clinopyroxene and Fe-Ti oxides are listed.

In Fig. 13 the FeO and MgO content of olivine indicate a large compositional range. The MgO-rich olivines (upper left) are about fo90 and represent a large phenocryst in olivine tholeiite sample MS31-70 (Table 4) and xenocryst in sample MS38-78 (Table 4) from Kerlingarhraun, the most recent lava on Melrakkaslétta. The most iron rich composition of fo34 represents a small groundmass olivine from the same sample. The majority of the microphenocrysts and groundmass crystals fall between fo75 and fo52 as commonly observed in tholeiitic basalts.

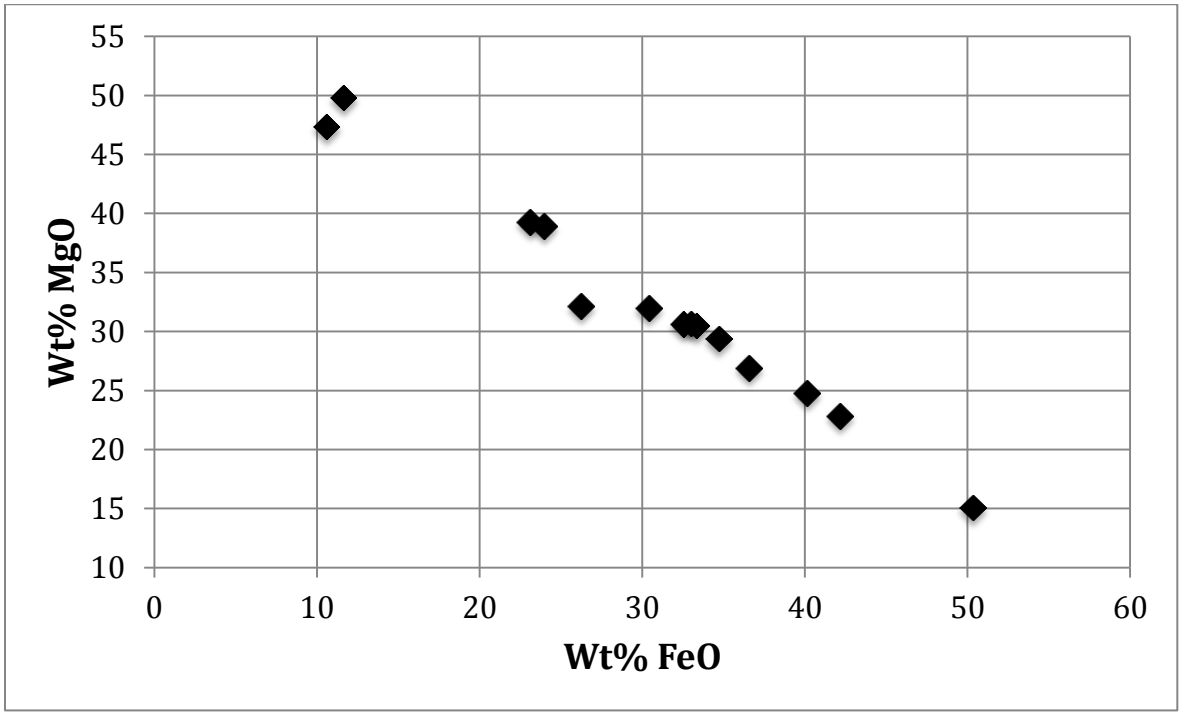

Fig. 13 Olivine composition.

Compositions of olivine in the Melrakkaslétta samples cover the whole range of olivines reported from rift-zones in Iceland. However, the most magnesian olivines are either xenocrysts in tholeiites or large phenocrysts from the most magnesian lavas from the western margin of Melrakkaslétta.

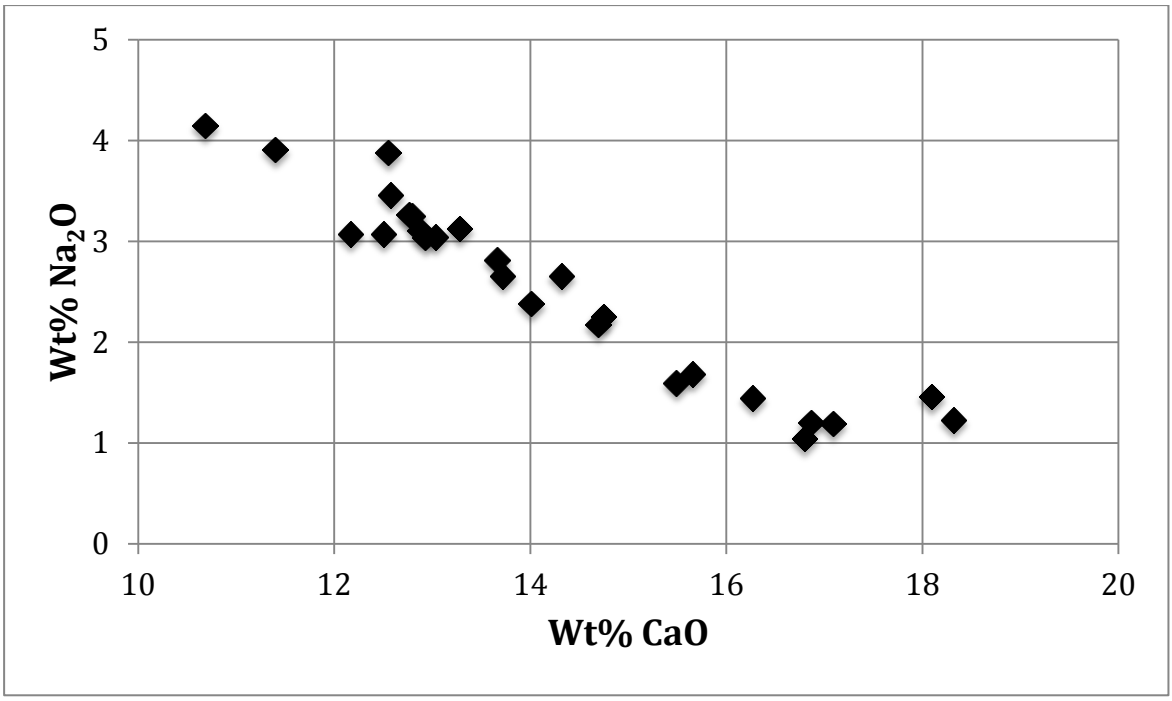

Fig. 14 Plagioclase composition.

In Fig. 14 the compositional range of plagioclase shows a continuum across the bytownite field. An exception to this is found in xenocrysts from samples MS7-34 and MS8-35 and in the large xenocrysts in sample MS31-70. These anorthite compositions are seen in the lower right of the Figure. The most evolved groundmass plagioclase, at the bytownite-labradorite boundary are found in sample MS8-35 (oldest formation) and in sample MS30-66 from the youngest lava (Table 5). The compositional range of plagioclase may be interpreted as the result of cotectic crystallization with olivine. The labradorite composition (upper left in Fig. 14) is found in groundmass at the ol-plag-cpx equilibrium and is assumed to represent the final stage of crystallization.

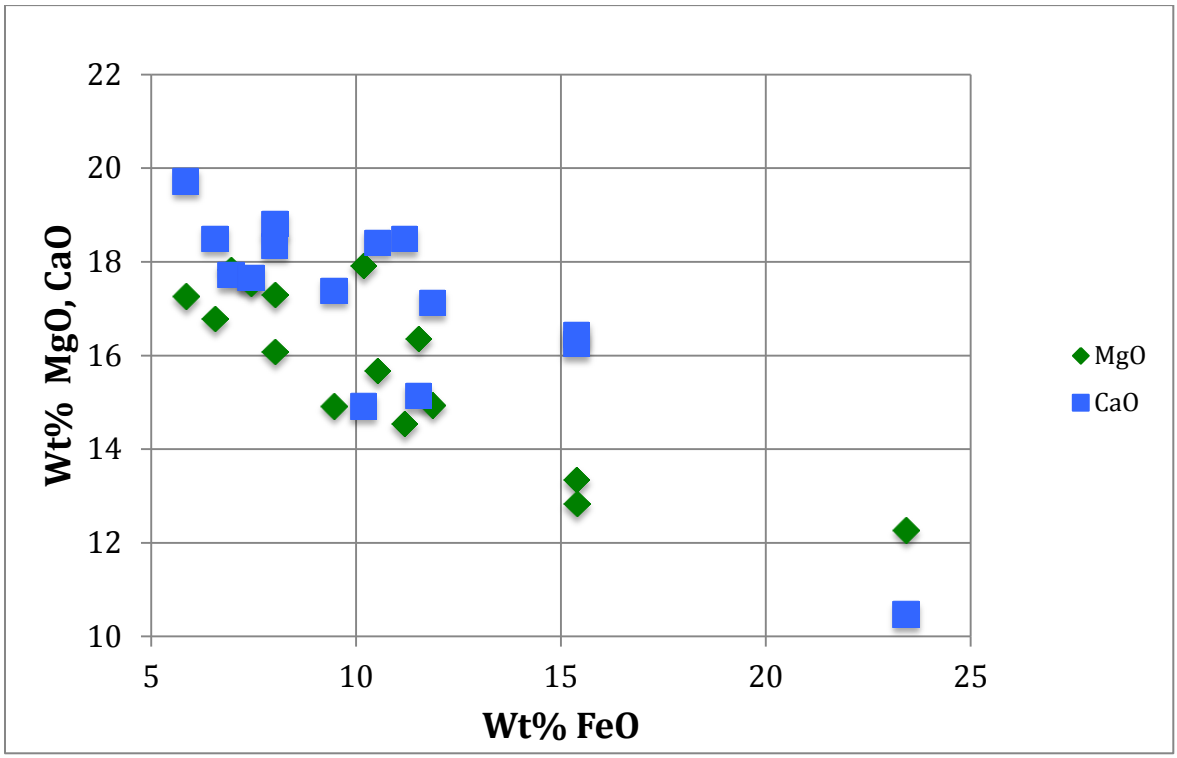

Fig. 15 Clinopyroxene composition.

MgO and CaO in clinopyroxene plotted against FeO is shown in Fig. 15. The most magnesian diopsides are from the porphyritic olivine tholeiite sample MS31-70 (Table 6) from the west margin of Melrakkaslétta. The compositions within the augite range trend towards composition Fs25.

In Fig. 16 the alumina content of the clinopyroxenes show a positive correlation with MgO. The crystals with the highest Al_2O_3 (samples MS8-35 and MS31-66) may be xenocrysts derived from pressure higher than average equilibration pressure of the Melrakkaslétta rocks. Crystals with similar MgO-content (16-18 Wt%) but lower Al_2O_3 content (less than 3%) may be assumed to be low pressure equivalents of the magnesian pyroxenes. This suggests that some of the magnesian clinopyroxenes may be xenocrysts.

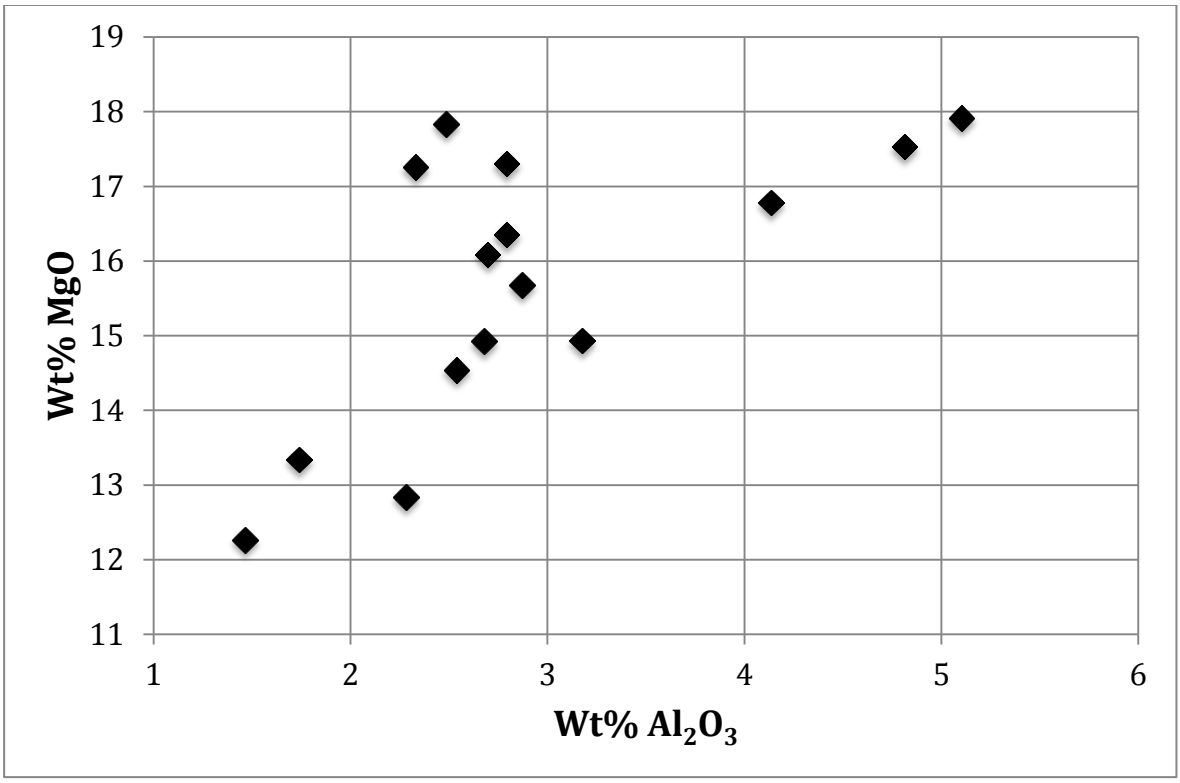

Fig. 16 MgO vs. Al_2O_3 in clinopyroxene.

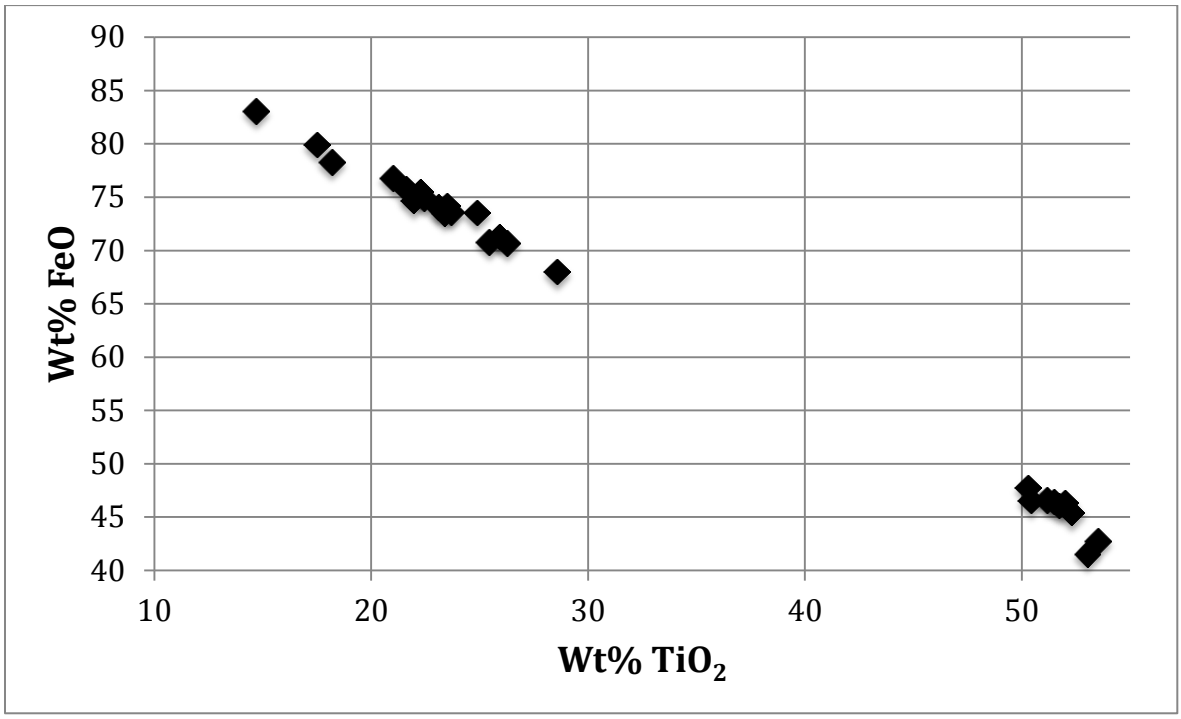

Fig. 17 Fe-Ti oxide composition.

In Fig. 17 the FeO-TiO_2 relation of the Fe-Ti oxides illustrates the large compositional range of the titanomagnetite (upper left in the Figure) and the corresponding compositional variation of the ilmenite (lower right in the Figure). Titanomagnetite ranging from 78-40 Wt% in the ulvospinel component (Table 7) reflects the different TiO_2 content of the host magma. In table 7, equilibrium temperature for two mt-im pairs is calculated at 763 and 899°C respectively. This indicates that the oxides were equilibrating at temperatures approaching the Curie-point of the titanomagnetite at about 700°C. It is therefore concluded that the oxide mineralogy of the Melrakkaslétta basalts may largely depend on the cooling history of the lavas and may, accordingly, have limited significance in tracing the ultimate origin of these rocks.

4 Discussion

4.1 Petrochemistry of Melrakkaslétta

Chemical analyses of rocks from the Melrakkaslétta peninsula (Fig. 2) are listed in Tables 2 and 3. In terms of Large Ion Lithophilic Elements (LILE) such as Ba and High Field Strength Elements (HFSE) such as Zr the Melrakkaslétta basalts define a linear trend (Fig. 18). In crystal fractionation modeling the LILE five times enrichment from the lowest to the highest abundances would correspond to 80% fractionation. Since that degree of fractionation would force the melt well into the range of intermediate rocks it may be concluded that the trend in Fig. 18 shows at least two basalt types.

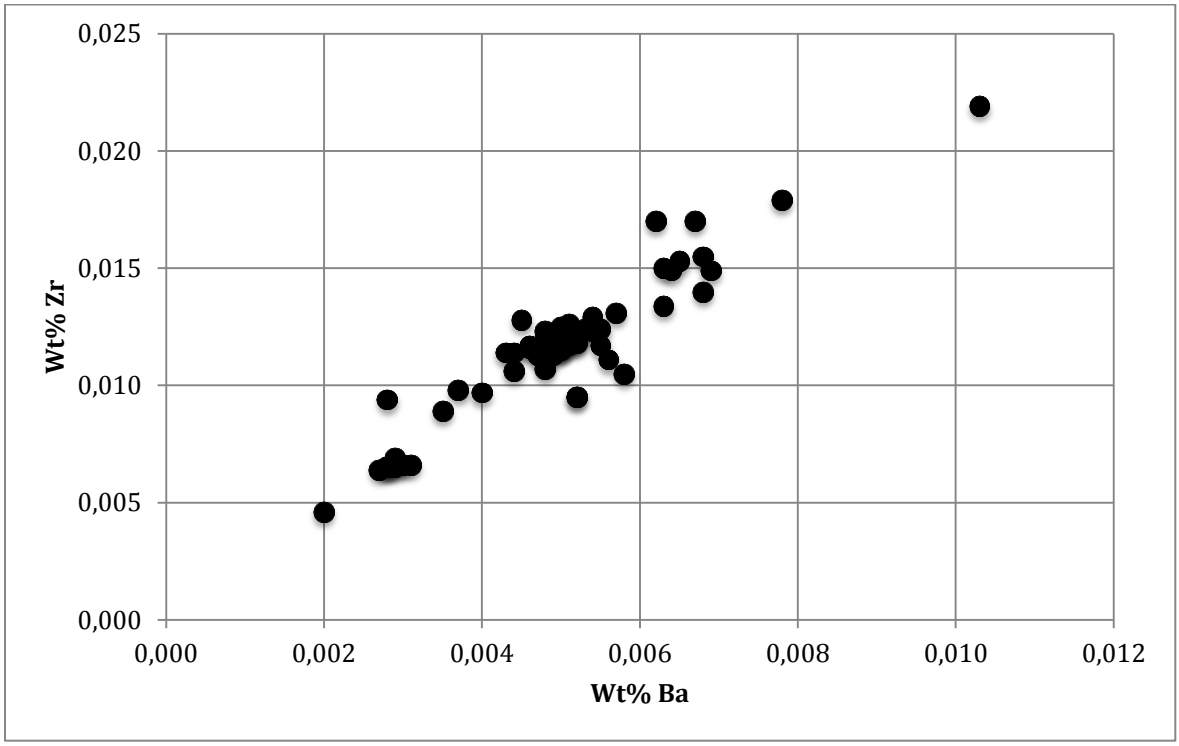

Fig. 18 Zr-Ba relations in the Melrakkaslétta basalts.

It may be stated that the low LILE basalts represent primitive olivine tholeiites while the central group of the trend represents tholeiites that may be the source of the high LILE basalts that range up to about 0.01 Wt% Ba (100 ppm).

High Field Strength Elements (Sun, Nesbitt, & Sharaskin, 1979) such as Zr and Ti are essentially small ions with high charge that during partial melting enter the melt at early stages and at comparable rates due to similar distribution coefficients between a melt and the major mantle phases (gr, opx cpx and ol). In Fig. 19 the Zr-Ti relations in the Melrakkaslétta basalts are similar to the Zr-Ba trend.

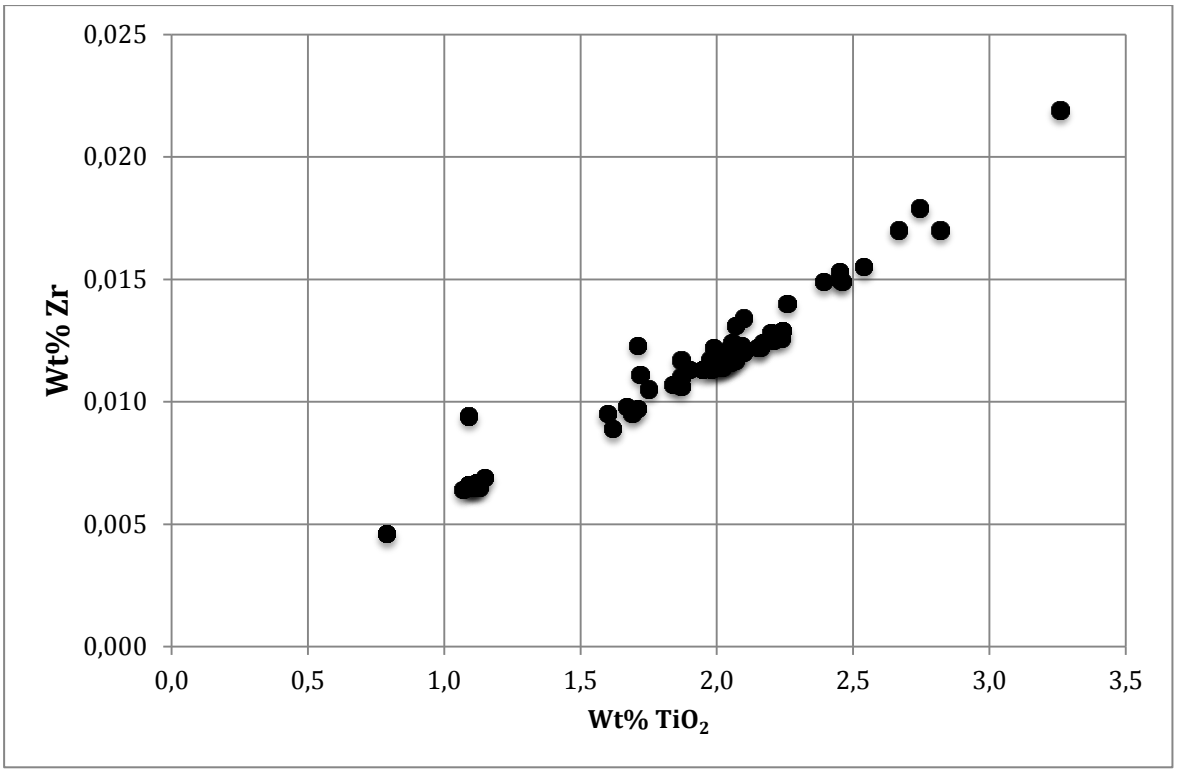

Fig. 19 Zr-Ti relations of the Melrakkaslétta basalts.

Figures 18 and 19 may indicate that the Melrakkaslétta basalt groups were produced by quite different degrees of partial melting in the mantle, as indicated by TiO_2 contents ranging from about 1 for the olivine tholeiites to about 2 for the tholeiite group.

Major element relations of the Melrakkaslétta basalts also indicate at least twofold origin; aluminous, low iron olivine tholeiite group and an iron rich tholeiite group (Fig. 20). These groups are composed of the same samples as the LILE and HFSE groups depicted in Figures 18 and 19.

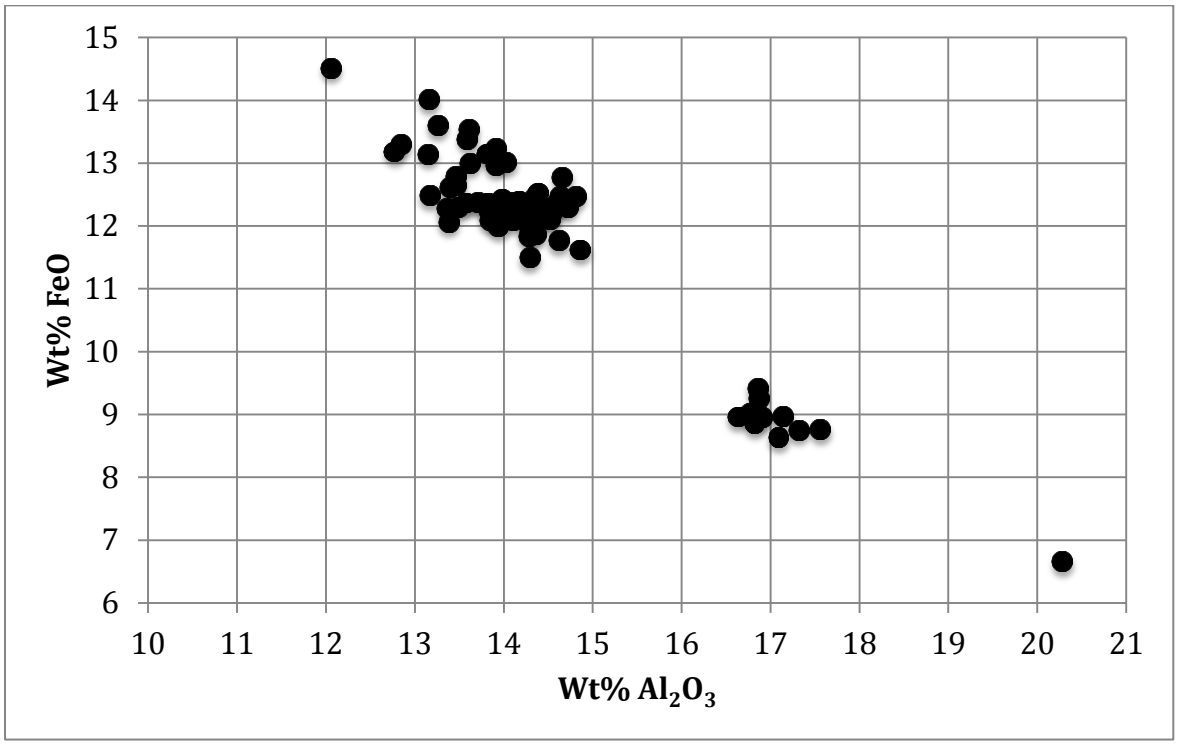

Fig. 20 Fe-Al relations of the Melrakkaslétta basalts. Note the high-Al sample in the lower right which represent olivine tholeiite with abundant plagioclase megacrysts.

Compatible trace elements such as Cr and Ni that might be expected to be related to the initial clinopyroxene and olivine component of the basaltic melt are shown in relation to Mg in Fig. 21. Nickel that may reflect the amount of mantle olivine melted shows a trend from the primitive olivine tholeiite (green, upper right in Fig. 21) towards low values in the tholeiites and their slightly evolved derivatives.

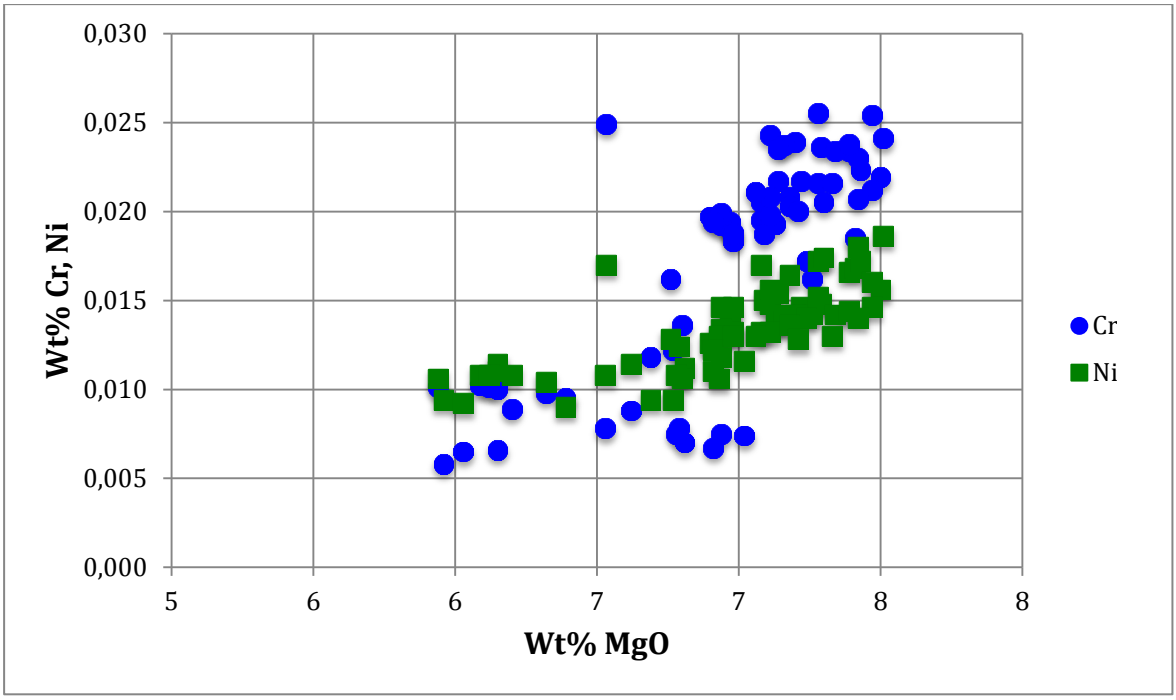

Fig. 21 (Cr, Ni)-Mg relations in the Melrakkaslétta basalts.

Chromium shows two basalt-groups that resemble the groups seen for the LILE and HFSE elements. Assuming that chromium (blue dots in Fig. 21) in spinel lherzolite is preferentially contained in the cpx it may be inferred that the high-Cr olivine tholeiite group contains a significantly larger share of melted cpx as compared with the low-Cr tholeiites. This melting scenario is essentially the same as suggested for the LILE and HFSE elements.

There is no doubt that the Melrakkaslétta basalts evolve on the An-Fo cotectic boundary within the Fo-Di-An phase system (Presnall, et al., 1978) and accordingly the expected trend between Ca and Mg reveals the relative share of plagioclase and olivine in the rocks. The high Ca abundance in the olivine tholeiite group shown in Fig. 22 is associated with significantly lower Fe-content (Table 2) as commonly observed in MORB (Mid Ocean Ridge Basalt). A trend between Ca and Mg within the tholeiite group may, indeed, represent crystal fractionation on the An-Fo cotectic.

In Fig. 22 open brown squares represent samples of brown hylaoclastite tuff. The commonly observed leaching of Ca during alteration of basaltic glass in the zeolite facies is very likely responsible for the deviation of the tuff towards lower Ca.

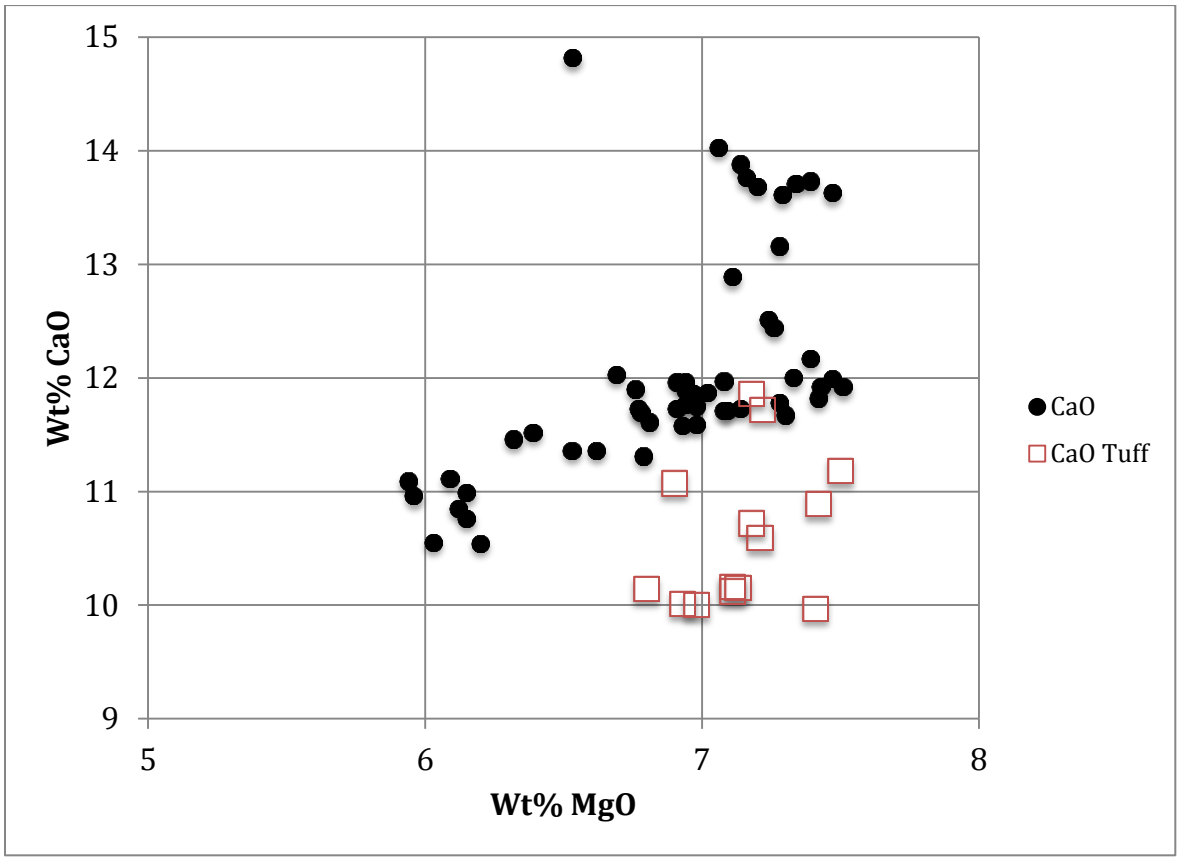

Fig. 22 Ca-Mg relations of the Melrakkaslétta basalts. Note the open rectangles that represent brown hyaloclastite tuff that has suffered extensive leaching of Ca.

Leaching of basaltic glass at oxidizing surface conditions would inevitably also affect abundance of vanadium that otherwise would show strong correlation with iron. In Fig. 23 the V-Fe relations of the Melrakkaslétta basalts show the same assumed leaching effect as the Ca-Mg relations. This may be taken as a strong evidence for leaching of hyaloclastite at shallow, oxidizing conditions that favor the formation of vanadium oxyanions and their mobility. Both Nickel and Chromium may be expected to show similar mobility but since these metals reside in ferromagnesian minerals their dissolution rate is far less than that of vanadium which resides in the volcanic glass that suffers quick postmagmatic alteration.

Tuff samples were not deleted from Tables 2 and 3 since the other more residual elements may still give useful information. These samples are, however, recorded in *italics* in Table 2 and 3.

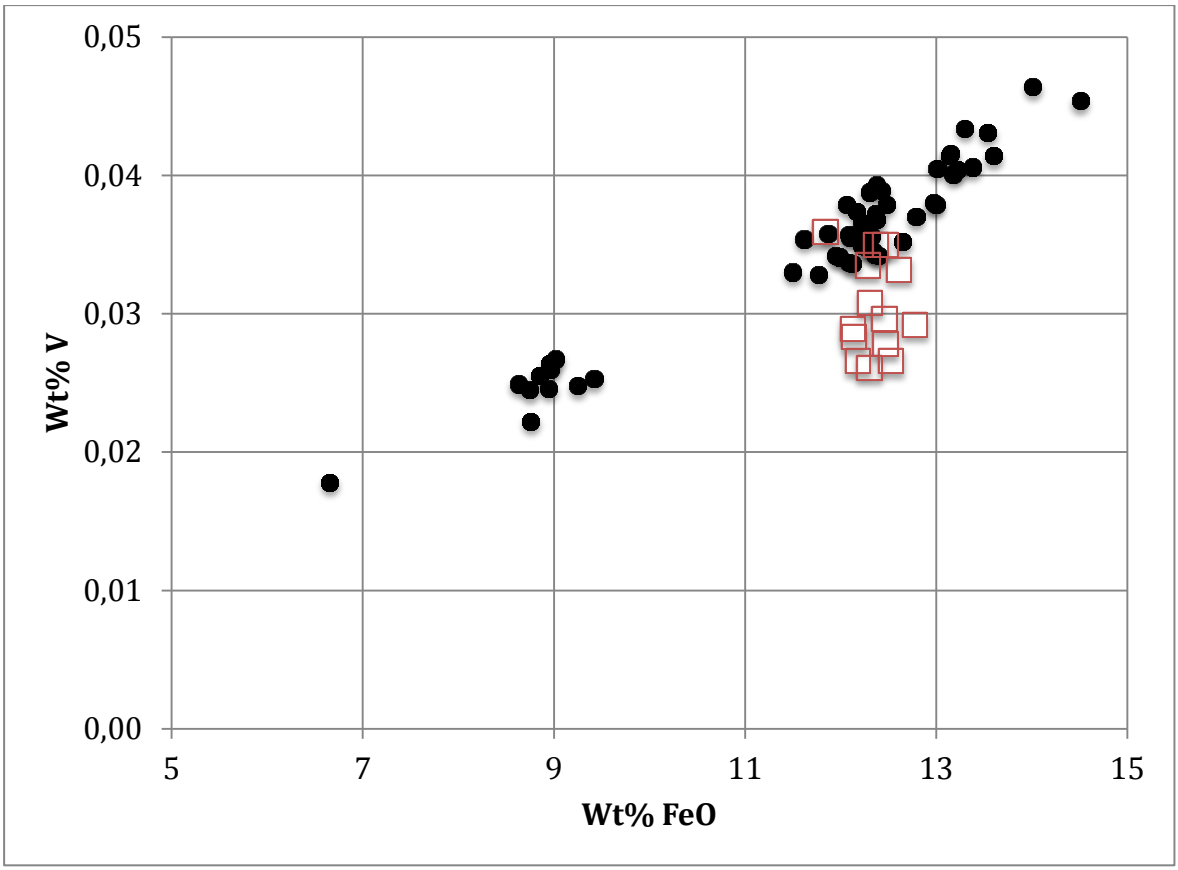

Fig. 23 V-FeO relations of the Melrakkaslétta basalts. Note the open rectangles that represent brown hyaloclastite tuff that has suffered extensive leaching of V.

Phosphorous that behaves like the HFSE in the olivine tholeiite-tholeiite rock suite seems to be generally enriched relative to the other HFSE in Fe-Ti basalts and high-Ti basalts on rift margins, such as the Kverkfjöll volcanic lineament. Among the Melrakkaslétta rocks a series of samples, indeed, show this trend, being higher in phosphorus relative to Ti as compared with the tholeiitic series.

In Fig. 24 this property may be seen as a compositional trend that separates from the far more common tholeiites. Here, this group of samples is noted as High-P tholeiites since the series differ markedly from the more compositionally restricted Fe-Ti basalt group. In the Figure the High-P tholeiites form a trend that ranges downwards to Ti-values close to that of the common tholeiites although the phosphorus is still higher.

Mantle origin of these High-P tholeiites and Fe-Ti basalts in general is beyond the scope of the present contribution but the alignment of the P_2O_5-TiO_2 trend suggest formation by different degree of melting rather than crystal fractionation. This is based on the fact that the trend has large negative intercept at the P_2O_5-axis in Fig. 24.

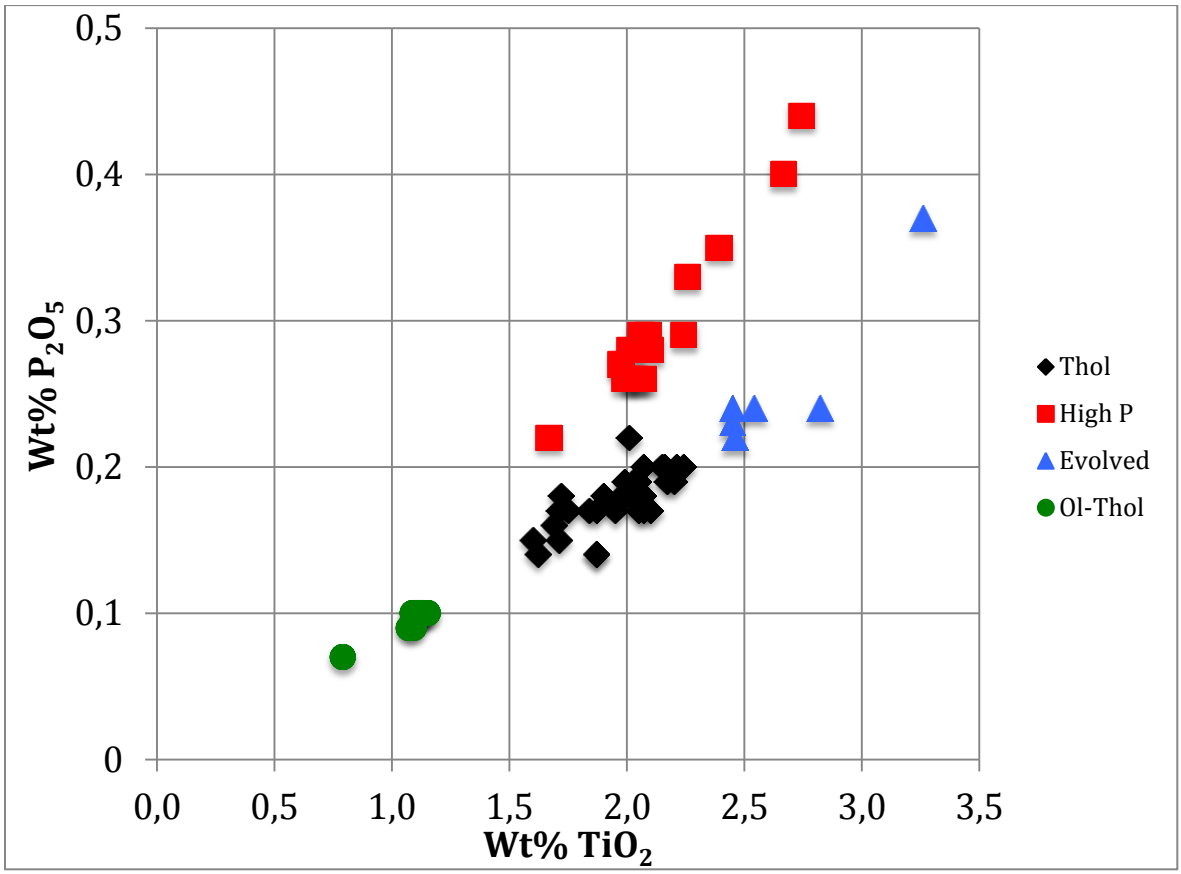

Fig. 24 P_2O_5-TiO_2 relations of the Melrakkaslétta basalts. Here the Melrakkaslétta basalts are divided into four groups; olivine tholeiites (green), common tholeiites (black), evolved tholeiites (blue) and High-P tholeiites (red).

To a first approximation the High-P rock series, including the Fe-Ti basalts, has to be derived from melting within a mantle segment of different mineralogy as compared with the tholeiite-yielding mantle beneath spreading ridges.

Phosphorus content of garnet (Breiter, Novák, Koller, & Cempírek, 2005) in lherzolite is variable but relatively high as compared with other mantle minerals. This relates to the bulk distribution coefficient of P (0,15-0,36) between garnet and its surroundings which is about three times higher than for olivine and pyroxene (Berlin, 2002), (Brunet, 2005). This may suggest that the High-P basalts are formed by melting where garnet is exhausted during the melting process. With reference to Fig. 24 it is unlikely that the High-P basalts are formed by higher degree of melting than the simultaneously produced tholeiites. Both basalt groups have comparable #Mg and indistinguishable LILE enrichment.

The remaining simple explanation may involve melting within the upper stability field of garnet, even within spinel lherzolite. In either case, the melting would consume and exhaust the garnet, yielding most of the phosphorus to the melt. The otherwise similar tholeiite and High-P groups thus differ in their source mineralogy, the High-P group being of shallower origin. This scenario might also suggest that the High-P group would occur locally where melting conditions migrate upwards due to tectonic causes.

Evolution of the tholeiite group and High-P group during crystal fractionation at low pressures such as fractionation within a slow flowing lava is largely similar until

precipitation of oxides sets in. Ilmenite might be expected to form more readily in the Ti-rich High-P group as well as formation of apatite which, however, was not observed in the present work.

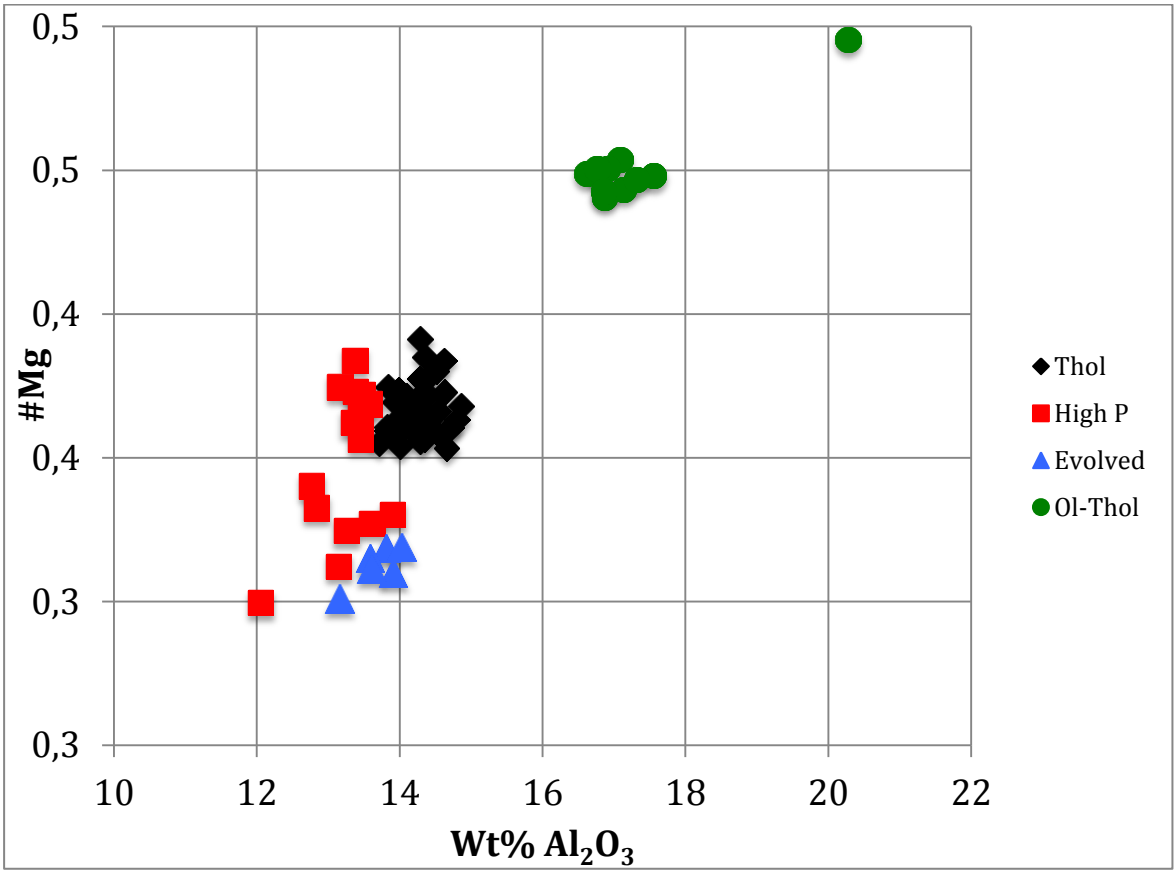

Fig. 25 #Mg-Al_2O_3 relations of the Melrakkaslétta basalts. The color-coding is the same as in Fig. 24.

In Fig. 25 the relations among the magnesium number and alumina in the Melrakkaslétta basalts are shown in relation to the grouping based on P-Ti relations. This Figure outlines the dual grouping of the Melrakkaslétta basalts. In the first place there is the obvious grouping, based on major elements, into olivine tholeiite and tholeiite. Then there is the group of evolved basalts which is assigned to low pressure fractionation as manifested by the fact that samples from the Holocene Kerlingarhraun fall into both the tholeiite group and the evolved group, the evolved members being cryptocrystalline lava groundmass.

The High-P group evolves aside the tholeiite group at slightly lower alumina levels which might be explained by melting within a mantle domain where the principal Al-host of the mantle, garnet, was low or absent making the more stable spinel phase the primary Al-host of the mineral assemblage. This mantle domain may also be characterized by high alumina content of clinopyroxene.

A conclusion based on the above discussion of rock chemistry is that basalt from three distinct magma sources are exposed on Melrakkaslétta.

4.2 Melrakkaslétta rocks and the regional petrology

Composition of the Melrakkaslétta basalts reveals at least two rock suites; olivine tholeiite and tholeiite. In Fig. 26 the P_2O_5-TiO_2 relations of the Melrakkaslétta basalts are shown in comparison with basalts from the Fjallgardar volcanic ridge (Helgason, 1989) and off-shore dredged samples from the GOR (Mertz, Devey, Todt, Stoffers, & Hofmann, 1991).

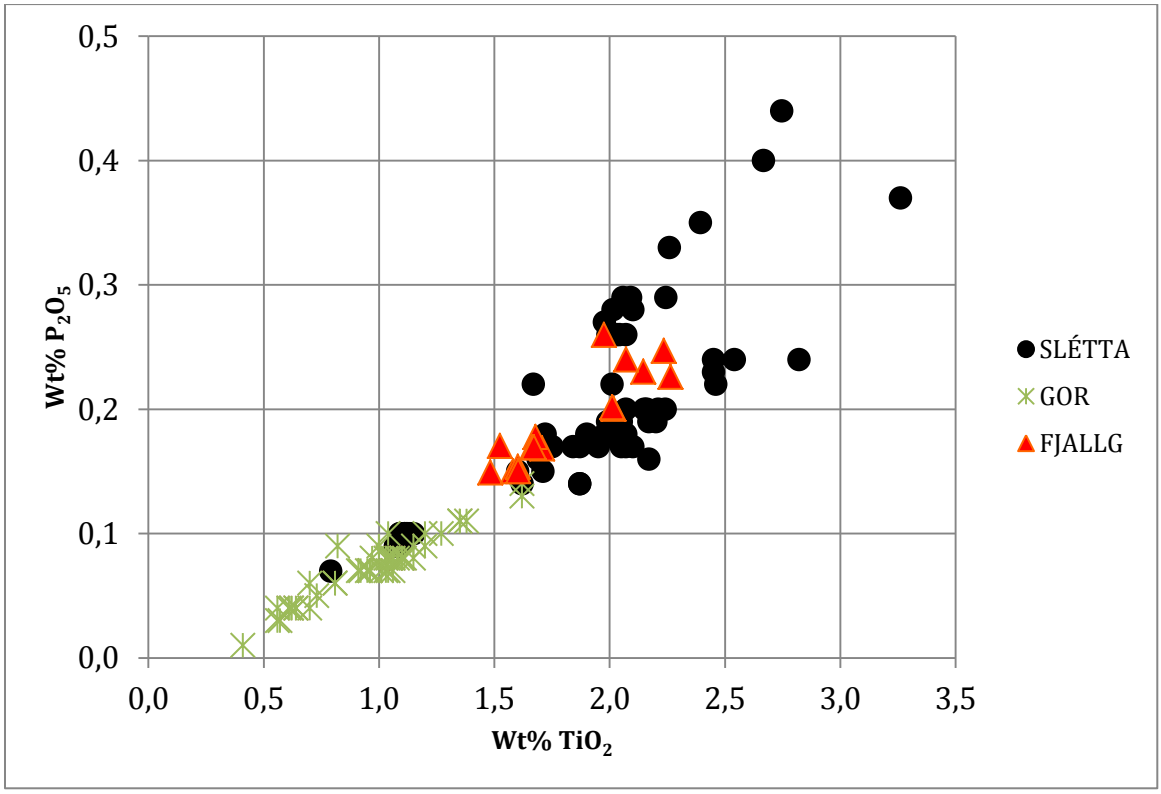

Fig. 26 P_2O_5-TiO_2 relations of the Melrakkaslétta basalts in comparison with basalts from adjacent formations.

There can be no doubt that the olivine tholeiite samples of Melrakkaslétta are members of the GOR rock suite denoted by green stars in Fig. 26. It is also noted that two of the GOR samples plot within the tholeiite field at 1.6% TiO_2. Red triangles in Fig. 26 represent samples from the Fjallgardar volcanic ridge (Helgason, 1989) that plot within the tholeiite field with one sample falling within the High-P group. Helgason (1989) noted the occurrence of the high-Ti rocks in the Fjallgardar basalts suite and classified two out of 42 samples as Fe-Ti basalt. It is clear that this Fe-Ti basalt classification is based on samples with more than 3 Wt% TiO_2 which in this is study are grouped as evolved tholeiites.

Fjallgardar is a subglacial volcanic ridge that during its formation defined the eastern margin of the Northern Rift Zone (NRZ). The present hypothesis that the High-P group is a subset of the tholeiite group that was generated at slightly lower pressures within spinel lherzolite suggests that these rocks may be generated within any rift margin provided that the thermal regime reaches into the spinel lherzolite. These conditions are therefore expected to arise where thermal gradient of a rift margin is raised by a new volcanic lineament or by anomalous local volcanism and intrusive activity.

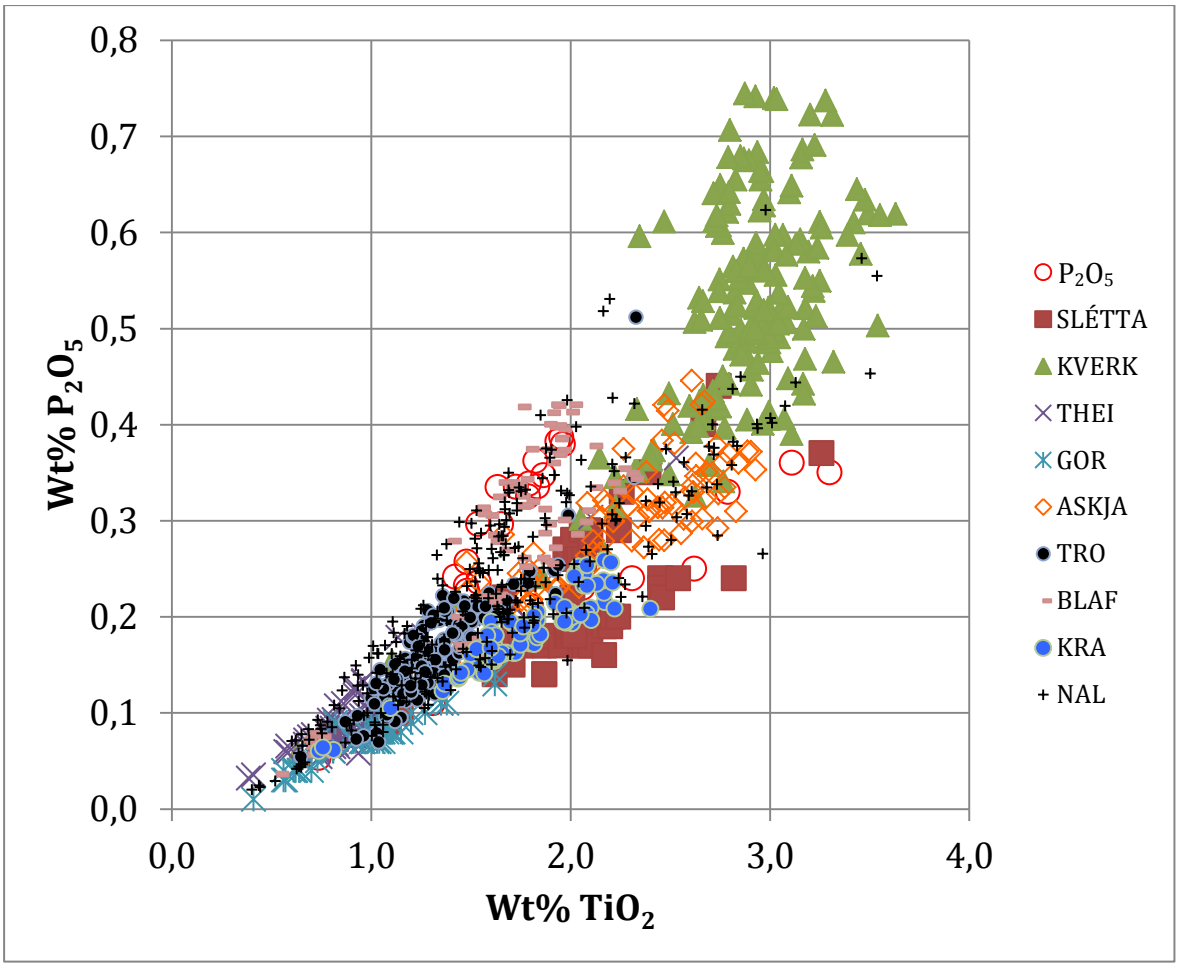

Fig. 27 P_2O_5-TiO_2 relations of the Melrakkaslétta basalts (Red squares) in comparison with basalts from the Northern Rift Zone of Iceland (NRZ). Legends of the Figure: P_2O_5 samples from the NRZ that are not assigned to a specific volcanic system, SLÉTTA refers to samples of the present study, KVERK refers to the Kverkfjöll volcanic system, THEY refers to the Theistareykir volcanic system, GOR refers to off-shore samples from the Grímsey Oblique Rift (Mertz, Devey, Todt, Stoffers, & Hofmann, 1991). ASKJA refers to samples from the Askja volcanic system (Sigvaldason G. E., 1974) TRO refers to samples from the Trölladyngja lava shield. BLAF refers to samples from the Bláfjall table mountain, KRA refers to samples from the Krafla volcanic system **(Nicholson, 1991)***; (Jónasson, 1994) and NAL refers to samples collected along the NRZ (Sigvaldason G. E., 1969).*

In regional context, the formation of the High-P group would be expected at rift zone margins and definitely above propagating rifts where upwards migration of thermal anomalies is inevitable.

Basalts of the olivine tholeiite series that characterize the GOR samples are found sporadically along the entire Icelandic rift system. However, their frequency is highest within the Theistareykir volcanic system (Slater, McKenzie, Grönvold, & Shimizu, 2001) where they dominate the basalt formation. There is no doubt that the olivine tholeiites on Melrakkaslétta represent this "normal oceanic" magma source that is assumed to be produced by high degree of mantle melting.

Among basalts from the NRZ the olivine tholeiites of Melrakkaslétta resemble basalts from the Theistareykir volcanic system, the tholeiites resemble basalts from the Krafla and

Fjallgardar volcanic systems and the High-P basalts resemble basalts from the Kverkfjöll volcanic system. In Fig. 27 where basalts from the data bank of the Nordic Volcanological Centre are plotted in terms of P_2O_5 and TiO_2 these mainlines of the Melrakkaslétta basalt-composition show that the tholeiites are relatively low in P_2O_5. It may be suggested that the volcanic systems that define the northern termination of the rift-zone, such as Krafla and Theistareykir, are generally more primitive in terms of LILE and HFSE as compared with the inland systems such as Askja.

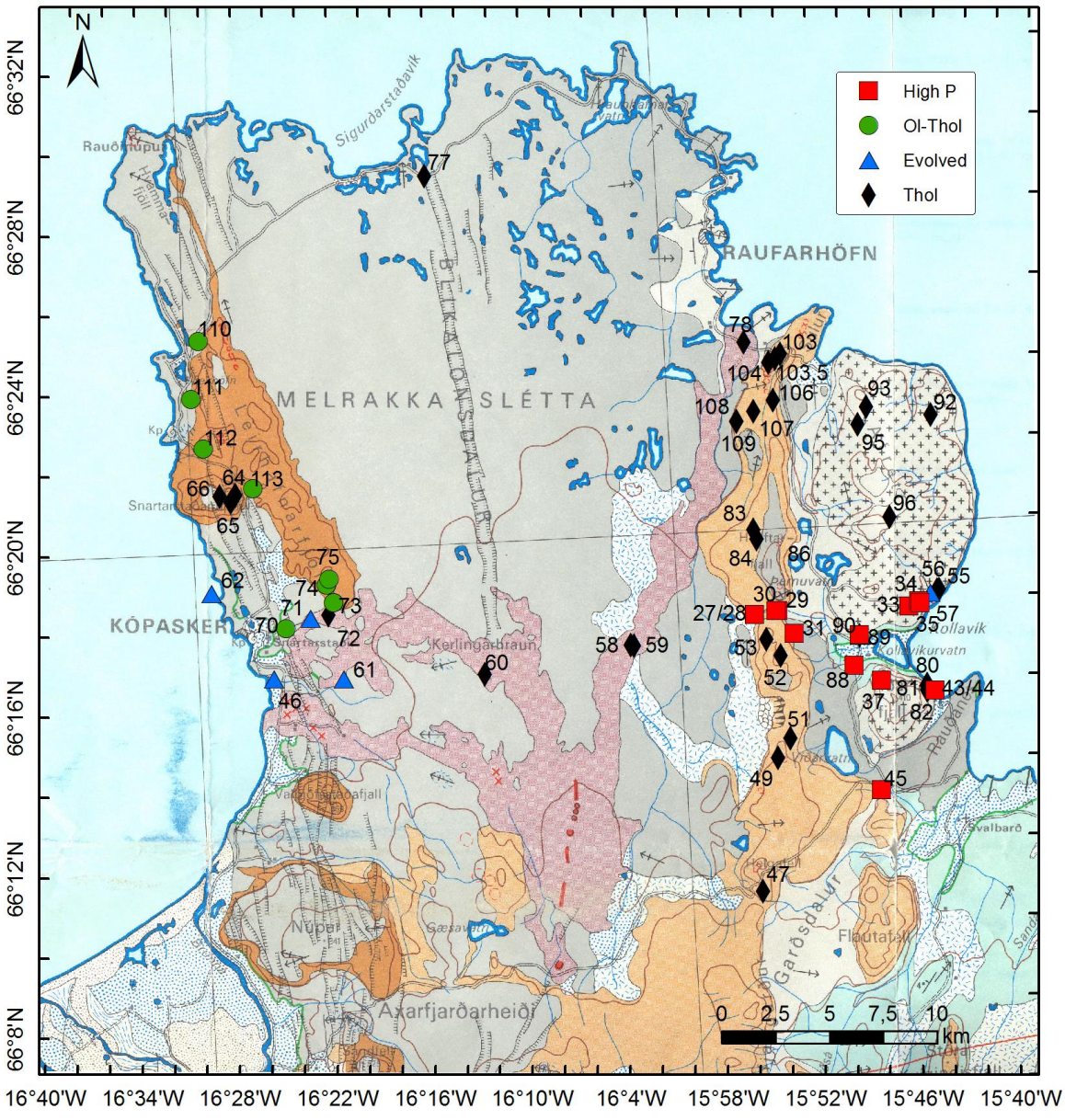

Fig. 28 Distribution of the four different rock types of Melrakkaslétta. The numbers represent the latter number of the sample names, see e.g. Table 2. The map is from (Sæmundsson, 1977), see legend in Fig. 2.

Formation of the Melrakkaslétta peninsula can be traced beyond the Brunhes-Matuyama magnetic reversal 0.78 my ago. These oldest rock outcrops are in the SE-margin of the peninsula and reach as far north as Krossavík (Fig. 2).

The two following subglacial formations separated by basaltic lava sequence reached farther north on the west margin of the initial formation. It is, therefore, concluded that the peninsula has been widening towards the west by successive formation of volcanic lineaments from the inland. The initial volcano-tectonic alignment of these systems are parallel to the more recent Blikalónsdalur graben in the center of the peninsula, with a N fracture orientation (160-59°) (Hjartardóttir, Einarsson, Magnúsdóttir, Björnsdóttir, & Brandsdóttir, 2014). This indicates that the crustal stress field of the peninsula was stable until the last glaciation when the subglacial formation along the west coast of Melrakkaslétta was formed. Basalts of these volcanic lineaments belong to the tholeiite basalt group with the local exception where High-P basalts were erupted.

Occurrence of the High-P basalt group is confined to local activity in the SE that ranges in age from the oldest to next-youngest hyaloclastite formations, presumably representing the Holstein and Weichselian epochs. It is suggested here that the local occurrence of High-P basalts during the early stages of the Melrakkaslétta peninsula results from a long standing thermal anomaly at the north termination of the initial Melrakkaslétta volcanic system. Such thermal anomaly associated with intense intrusive activity is assumed to have favored relatively shallow melting within spinel lherzolite that is the favored origin of the High-P basalts. The whole scenario may be looked upon as a short local rift propagation giving rise to magmas that in many respects resemble the Fe-Ti basalts of propagating rifts.

Olivine tholeiites of Melrakkaslétta are confined to the volcanic lineament along the most recent western margin of the peninsula. This lineament is aligned with NNW fracture orientation (110-159°) (Hjartardóttir, Einarsson, Magnúsdóttir, Björnsdóttir, & Brandsdóttir, 2014) in a striking contrast to the regionally prevailing fissure alignment.

There is no doubt that the olivine tholeiite volcanism is confined to the youngest hyaloclastite formation on the western margin of Melrakkaslétta. Although the common tholeiite basalts are also erupted along this lineament it has to be concluded that the olivine tholeiites are derived from the same mantle melting regime as the identical dredged GOR basalts (Fig. 26).

Recently discovered transform-tectonics on the SW margin of Melrakkaslétta (Hjartardóttir, Einarsson, Magnúsdóttir, Björnsdóttir, & Brandsdóttir, 2014) indicate that the local stress field along the west margin of Melrakkaslétta is associated with eastwards impact of the GOR. There is no doubt that this tectonic scenario created a new volcanic lineament that connects with the oceanic melting regime that feeds the off-shore volcanism.

In terms of crustal spreading the 30 km wide Melrakkaslétta peninsula corresponds to the half-width of the ocean floor spreading (2 cm/yr.) during the entire Quaternary period. However, the volcanic lineaments on Melrakkaslétta indicate strong but periodic spreading activity during significant rifting events.

5 Concluding remarks

Detailed sampling and analysis of rocks from the different volcanic lineaments of Melrakkaslétta reveals three rock types: a) Tholeiitic basalts that dominate the oldest volcanic lineaments in the eastern half of the peninsula and the dolerite lava fields covering the central peninsula. b) Evolved high phosphorous basalts with strong Fe-Ti affinities occurring locally among the older rocks in the SE-part of the peninsula and c) olivine tholeiites that occur along the west coast of the peninsula.

The tholeiite suite is in most respects similar to the tholeiitic rock suite of the Krafla volcanic system to the west. The high phosphorous group resembles moderately evolved rocks from the Kverkfjöll volcanic system to the south while the olivine tholeiites along the west coast resemble olivine tholeiites dredged off-shore to the north and west of Melrakkaslétta.

Formation of Melrakkaslétta during the earliest Quaternary followed a northwards rift-propagation of an inland volcanic lineament with a N fracture orientation (160-59°) (Hjartardóttir, Einarsson, Magnúsdóttir, Björnsdóttir, & Brandsdóttir, 2014) as far north as Afrétt that defines the present SE-coast of the peninsula. During the Quaternary, successively younger parallel volcanic lineaments formed on the rift side (west) of earlier lineaments. The Fjallgarðar lineament reaches north parallel with Afrétt while at least one successive lineament, now mostly covered by dolerite lavas, probably reached as far north as Hraunhafnartangi.

Blikalónsdalur is a narrow recent tectonic graben along the center of the peninsula that cuts the central dolerite interglacial lava field, Blikalónsdalur is parallel to the earlier tectonic lineaments of Melrakkaslétta. A productive volcanic lineament formed during the last glaciation along the west coast of the peninsula. Although the common tholeiites of Melrakkaslétta are frequently erupted along the west coast the recent volcanic lineament is characterized by olivine tholeiites matching the composition of the off-shore volcanism. This youngest volcanic lineament with a NNW fracture orientation (110-159°) (Hjartardóttir, Einarsson, Magnúsdóttir, Björnsdóttir, & Brandsdóttir, 2014) is subparallel to all other volcanic structures of the peninsula and its south-termination is connected to the junction of the presently active rift-zone and the GOR that runs into Melrakkaslétta from the north-east in Núpasveit.

References

Albertsson, K. J., Guðjónsson, G., Pétursson, H. G., Kristinssin, H., Jónsson, H. B., Nielsen, Ó. K., et al. (2003). *Norðausturvegur um Melrakkasléttu - Náttúrufarskönnun vegna vegagerðar.* Náttúrufræðistofnun Íslands. Akureyri: Náttúrufræðistofnun Íslands.

Buddington, A. F., & Lindsley, D. H. (1964). Iron-titanium oxide minerals and synthetic equivalents. *Journal of Petrology , 5*, 310-357.

Berlin, J. (2002). Phosphorus equilibria among mafic silicate phases - Abstract. *Denver Annual Meeting (October 27-30, 2002).* Denver: The Geological Society of America (GSA).

Brunet, F. (2005). Phosphorus, a Minor Element to Track UHP conditions: an Experimental Insight. *American Geophysical Union, Fall Meeting 2005, abstract #V51E-06.).*

Breiter, K., Novák, M., Koller, F., & Cempírek, J. (2005). Phosphorus - an omnipresent minor element in garnet of diverse textural types from leucocratic granitic rocks. *Mineralogy and Petrology , 85* (3-4), 205-221.

Einarsson, P., & Sæmundsson, K. (1987). Earthquake epicenters 1982-1985 and volcanic systems in Iceland (map). (T. Sigfússon, Ed.) *Í hlutarins eðli: Festschrift for Þorbjörn Sigurgeirsson* , Reykjavík: Menningarsjóður.

Hansen, H. H. (2010). *Atlaskort 29.* Reykjavík: Mál og menning.

Hartley, M. E., & Thordarson, T. (2013). The 1874-1876 volcano-tectonic episode at Askja, North Iceland: Lateral flow revisited. *Geochem. Geophys, Geosyst. , 14*, 1-24.

Helgason, J. (1987). *Jarðfræðirannsóknir á vatnasviði Jökulsár á Fjöllum við Möðrudal.* Orkustofnun, Vatnsorkudeild. Reykjavík: Orkustofnun.

Helgason, J. (1989). The Fjallgardar volcanic ridge in NE Iceland: an aborted early stage plate boundary or a volcanically dormant zone? (A. D. Norry, Ed.) *Magmatism in the Oceans Basins, Geol. Soc. Spec. Publ. , 42*, pp. 201-213.

Hjartardóttir, Á. R., Einarsson, P., Magnúsdóttir, S., Björnsdóttir, Þ., & Brandsdóttir, B. (2014). Fracture systems of the Northern Volcanic Rift Zone, Iceland - an onshore part of the Mid-Atlantic plate boundary. *Geological Society of London, Special Publications, in press* .

Jóhannesson, H., & Sæmundsson, K. (2009). *Geological map of Iceland. Bedrock geology.* Icelandic Institute of Natural History. Reykjavík: Icelandic Institute of Natural History.

Jóhannesson, H., & Sæmundsson, K. (2009). *Geological map of Iceland. Tectonics.* Icelandic Institute of Natural History. Reykjavík: Icelandic Institute of Natural History.

Jónasson, K. (1994). Rhyolite Volcanism at the Krafla Central Volcano, NE Iceland. *Bulletin of Volcanology , 56*, 516-528.

Lepage, D. L. (2014). ILMAT: A Magnetite-Ilmenite Geothermobarometry Program (version 1.20c). *Lepage@geoladm.geol.queensu.ca* .

Nicholson, H. (1991). *The magmatic evolution of Krafla, NE Iceland.* PhD thesis. Edinburgh: University of Edinburgh.

Mertz, D. F., Devey, C. W., Todt, W., Stoffers, P., & Hofmann, A. W. (1991). Sr-Nd-Pb isotope evidence against plume-asthenosphere mixing north of Iceland. *Earth and Planetary Science Letters , 107* (2), 243-255.

Pétursson, H. G. (1979). *Jarðfræði Núpasveitar.* Háskóli Íslands, Jarðfræðiskor. Reykjavík: Háskóli Íslands.

Pétursson, H. G. (1997). *Jarðfræðikönnun vegna sorpurðunar við Kópasker.* Náttúrufræðistofnun Íslands. Akureyri: Náttúrufræðistofnun Íslands.

Pétursson, H. G. (1986). *Kvartærgeologiske undersökelser på Vest-Melrakkasletta, Nordöst-Island.* Universitetet i Tromsö. Tromsö: Universitetet i Tromsö.

Pétursson, H. G., & Larsen, G. (1992). An early Holocene basaltic tephra bed in North Iceland, a possible equivalent to the Saaksunarvatn Ash Bed. In H. N. Áslaug Gerisdóttir (Ed.), *Abstracts: 20th Nordic Geological Winter Meeting, 7-10 January* (p. 133). Reykjavík: Jarðfræðafélag Íslands & Raunvísindastofnun Háskólans.

Pétursson, H. G., & Norðdahl, H. (1998). *Efnisleit á Hólaheiði á Melrakkasléttu.* Vegagerðin, Vegagerðin á Akureyri. Akureyri: Vegagerðin.

Presnall, D. C., Dixon, S. A., Dixon, J. R., O'Donnell, T. H., Brenner, N. L., Schrock, R. L., et al. (1978). Liquidus Phase Relations on the Join Diopside-Fosterite-Anotrhite From 1 atm to 20 kbar: Their Bearing on the Generation and Crystallization of Basaltic Magma. *Contrib. Mineral. Petrol. , 66*, pp. 203-220.

Sæmundsson, K. (1977). Geological map of Iceland Sheet 7 North East Iceland. Reykjavík: Iceland Geodetic Survey and the Museum of Natural History.

Sun, S.-S., Nesbitt, R. W., & Sharaskin, A. Y. (1979). Geochemical characteristics of mid-ocean ridge basalts. *Earth Planet. Sci. Lett.* (44), 119-38.

Sigvaldason, G. E. (1974). Basalts from the Centre of the Assumed Icelandic Mantle Plume. *Journal of Petrology , 15* (3), 497-524.

Sigvaldason, G. E. (1969). Chemistry of basalts from the Icelandic rift zone. *Contrib. Mineral. Petrol. , 20*, 357-370.

Slater, L., McKenzie, D., Grönvold, K., & Shimizu, N. (2001). Melt Generation and Movement beneath Theistareykir, NE Iceland. *Journal of Petrology , 42* (2), 321-354.

Thordarson, T., & Larsen, G. (2007). Volcanism in Iceland in historical time: Volcano types, eruption stykes and eruptive history. *J. Geodyn , 43*, 118-152.

Appendix I

Table 8. Description of hand samples, phenocryst determinations are coded as follows: Pl, plagioclase; Ol, olivine; Id, Iddingsite. Parentheses indicate phase present in small quantities (<1%).

Sample	Description	Phenocrysts	Magnetic polarity
MS1m-27	Dark grey brownish tuff, porous <0,5% d=0,5mm, coarse grained, irregular fractures, with bits of glassy rocks		Normal
MS1b-27	Dark grey, plagioclase 1-2% d=3mm, olivine <1% d=1mm porous 5% d=3mm, fine grained, irregular sharp fractures	Pl,(Ol)	
MS2-28	Hand sample missing		Normal
MS3-29	Grey, plagioclase 1% d=1mm, porous 10% d=2mm, small grained, irregular fractures	Pl	Normal
MS4-30	Light grey, plagioclase <1% d=1mm, porous 1-2% d=1mm, coarse grained, irregular sharp fractures	(Pl)	Normal
MS5-31	Grey, plagioclase 1-2% d=2mm, olivine <1% d=1mm, porous <1% d=1mm, small grained, irregular sharp fractures	Pl, (Ol)	Reverse
MS6-33	Grey, plagioclase <1% d=3mm, olivine <1% d=3mm, porous <1% d=1mm, small grained, irregular sharp fractures	(Pl), (Ol)	Reverse
MS7-34	Grey, plagioclase 1-2% d=2mm, olivine <1% d=1mm, porous <1% d=1mm, small grained, irregular sharp fractures	Pl, (Ol)	Reverse
MS8-35	Darkish grey, plagioclase <1% d=3mm, olivine < 1% d=2mm, porous 3% d=1mm, small grained, sharp fractures	(Pl), (Ol)	
MS9-37	Grey, plagioclase 1% d=2mm, olivine <1% d=1mm, porous <1% d=0,5mm, small grained, irregular sharp fractures	Pl, (Ol)	Reverse
MS10-43	Dark grey, porous <0,5% d=<0,5mm, fine grained, irregular sharp fractures		
MS11-44	Grey, plagioclase 1-2% d=5mm, olivine <1% d=1mm, porous 1-2% d=2mm, small grained, irregular sharp fractures	Pl, (Ol)	Normal
MS12-45	Dark grey, plagioclase <1% d=1mm, olivine <1% d=1mm, porous 2% d=1mm, small grained, irregular sharp fractures	(Pl), (Ol)	Normal
MS14-46	Grey, plagioclase 2-3% d=3mm, olivine <1% d=2mm, porous <1% d=1mm, small grained, irregular sharp fractures	Pl, (Ol)	
MS15-47	Dark grey, plagioclase 1-2% d=3mm, porous 25% d=3mm, small grained, irregular sharp fractures	Pl	
MS16b-49	Dark grey, plagioclase <1% d=2mm, porous 15% d=3mm, coarse grained, irregular fractures	(Pl)	

Table 8 (continued).

Sample	Description	Phenocrysts	Magnetic polarity
MS17-51	Hand sample missing		
MS18-52	Brown tuff, porous <0,5% d=0,5mm, coarse grained, irregular fractures, with bits of glassy rocks		
MS19-53	Brown tuff, porous <0,5% d=0,5mm, coarse grained, irregular fractures, with bits of glassy rocks		
MS20-55	Dark grey, plagioclase <1% d=1mm, small grained, irregular fractures		
MS21-56	Dark grey, plagioclase <1% d=1mm, small grained, irregular fractures		Reverse
MS22-57	Grey brownish, plagioclase <1% d=1mm, porous 1% d=3mm, small grained, irregular fractures, weathered	(Pl)	Normal
MS23-58	Dark grey, plagioclase <1% d=1mm, porous 20% d=4mm, fine grained, irregular sharp fractures	(Pl)	
MS24-59	Grey, plagioclase <1% d=0,5mm, porous 1% d=2mm, fine grained, irregular sharp fractures	(Pl)	
MS25-60	Dark grey, plagioclase <1% d=0,5mm, porous 20% d=8mm, fine grained, irregular sharp fractures, weathered	(Pl)	
MS26-61	Grey, plagioclase 2% d=3-4mm, olivine 1% d=2-3mm, cpx 0,5% d=2mm, porous <1% d=2mm, small grained, irregular sharp fractures	Pl, Ol	
MS27-62	Grey with a tint of red, plagioclase 3% d=3mm, olivine <1% d=1mm, porous <1% d=2mm, small grained, irregular sharp fractures	Pl, (Ol)	
MS28b-64	Dark grey, plagioclase <1% d=3mm, porous 2% d=1mm, fine grained, irregular fractures	(Pl)	
MS28m-64	Brown tuff, porous <1% d=0,5mm, coarse grained, irregular fractures, with bits of rocks		
MS29-65	Brown tuff, porous <1% d=0,5mm, coarse grained, irregular fractures, with bits of rocks		
MS30-66	Grey, plagioclase 1% d=3-4mm, olivine <1% d=1mm, porous <1% d=1mm, small grained, irregular sharp fractures	Pl, (Ol)	Normal
MS31-70	Grey brownish, plagioclase 60% d=15mm, iddingsite 1% d=2-3mm, porous <1% d=1mm, coarse grained, irregular fractures, weathered	Pl, Id	Normal
MS32-71	Grey, plagioclase 3-4% d=4mm, olivine <1% d=1mm, porous 1% d=2mm, small grained, irregular sharp fractures	Pl, (Ol)	Normal
MS33-72	Dark grey, plagioclase <1% d=0,5mm, porous 20% d=8mm, fine grained, irregular sharp fractures	(Pl)	
MS34b-73	Darkish grey, plagioclase 20% d=3-4mm, olivine < 1% d=2mm, porous 15% d=3mm, small grained, irregular sharp fractures	Pl, (Ol)	

Table 8 (continued).

Sample	Description	Phenocrysts	Magnetic polarity
MS34m-73	Brown tuff, plagioclase 1% d=5mm, olivine <1% d=1mm, porous <0,5% d=0,5mm, coarse grained, irregular fractures, with bits of glassy rocks	Pl, (Ol)	
MS35b-74	Darkish grey, plagioclase 1-2% d=1mm, porous 1% d=0,5mm, coarse grained, irregular fractures	Pl	
MS35m-74	Brown tuff, porous <0,5% d=0,5mm, coarse grained, irregular fractures, with bits of glassy rocks		
MS36-75	Brown tuff, porous 1% d=1mm, coarse grained, irregular fractures, with bits of glassy rocks		Normal
MS37-77	Light grey, plagioclase <1% d=1mm, porous <0,5% d=<0,5mm, small grained, irregular sharp fractures	(Pl)	Normal
MS38-78	Dark grey, porous 2% d=4mm, fine grained, irregular sharp fractures		Normal
MS39-80	Grey, plagioclase <1% d=2-3mm, porous in certain areas 3% d=2mm, small grained, irregular sharp fractures	(Pl)	Normal weak
MS40-81	Grey, plagioclase 2% d=3-4mm, olivine <1% d=1-2mm, porous 1% d=2mm, small grained, irregular sharp fractures	Pl, (Ol)	Reverse weak
MS41b-82	Grey, plagioclase 1% d=1-2mm, olivine 0,5% d=0,5-1mm, porous 2% d=2mm, small grained, irregular sharp fractures	Pl, (Ol)	
MS41m-82	Light brown tuff, porous <0,5% d=0,5mm, coarse grained, irregular fractures, with bits of glassy rocks		
MS42-83	Dark grey, plagioclase 1-2% d=3mm, olivine <1% d=1mm, porous 1% d=3mm, fine grained, irregular sharp fractures	Pl, (Ol)	Normal
MS43b-84	Darkish grey, plagioclase 1% d=1-2mm, olivine <0,5% d=0,5mm, porous 1% d=4mm, fine grained, irregular fractures	Pl, (Ol)	
MS43m-84	Brown tuff, porous <0,5% d=0,5mm, coarse grained, irregular fractures, with bits of glassy rocks		
MS45-88	Grey, plagioclase <0,5% d=<1mm, olivine <0,5% d=<1mm, porous <1% d=<1mm, small grained, irregular sharp fractures	(Pl), (Ol)	Reverse
MS46-89	Grey, plagioclase <1% d=1-2mm, olivine <1% d=1mm, porous <1% d=<1mm, small grained, irregular sharp fractures	(Pl), (Ol)	Normal
MS47fínt-90	Grey, plagioclase <1% d=1-2mm, olivine 1% d=2mm, porous <1% d=<1mm, small grained, irregular fractures	Ol, (Pl)	Reverse
MS47gróft-90	Grey, plagioclase <1% d=1-2mm, olivine 1% d=2mm, porous <1% d=<1mm, coarse grained, irregular fractures	Ol, (Pl)	

Table 8 (continued).

Sample	Description	Phenocrysts	Magnetic polarity
MS48-92	Grey, plagioclase 1% d=2mm, olivine 0,5% d=1mm, porous <1% d=1mm, small grained, irregular sharp fractures	Pl, (Ol)	Anomaly
MS49-93	Grey, plagioclase 1% d=2mm, olivine <0,5% d=1mm, porous <0,5% d=0,5mm, small grained, irregular sharp fractures	Pl, (Ol)	Reverse
MS50-95	Brown tuff, porous 0,5% d=1mm, coarse grained, irregular fractures, with bits of glassy rocks		
MS51-96	Grey, plagioclase 1% d=1-2mm, olivine 0,5% d=2mm, porous <1% d=<1mm, small grained, irregular fractures	Pl, (Ol)	Reverse
MS52-103	Dark grey brownish tuff, porous <0,5% d=1mm, fine grained, irregular sharp fractures, with bits of glassy rocks		
MS52,5-103,5	Grey, plagioclase 1% d=2mm, olivine 0,5% d=1mm, porous <1% d=1mm, small grained, irregular fractures	Pl, (Ol)	
MS53-104	Brown tuff, porous <0,5% d=0,5mm, coarse grained, irregular fractures, with bits of glassy rocks		
MS54-106	Brown tuff, porous <0,5% d=0,5mm, small grained, irregular fractures, with bits of glassy rocks		
MS55-107	Grey, plagioclase 1% d=2-3mm, olivine 0,5% d=1mm, porous <0,5% d=<0,5mm, small grained, irregular fractures	Pl, (Ol)	
MS56-108	Grey, plagioclase 1% d=2-3mm, olivine 0,5% d=1mm, porous 1% d=1mm, small grained, irregular fractures	Pl, (Ol)	
MS57-109	Dark grey brownish tuff, porous <0,5% d=1mm, fine grained, irregular sharp fractures, with bits of glassy rocks		
MS58-110	Grey, plagioclase 10% d=8mm, olivine <1% d=2mm, porous 15%, small grained, irregular fractures, a little weathered	Pl, (Ol)	
MS59-111	Dark grey, plagioclase 10% d=7mm, olivine 2-3% d=1-2mm, porous 10%, fine grained, irregular fractures	Pl, Ol	
MS60-112	Dark grey, plagioclase 10% d=8mm, olivine <1% d=2mm, porous 15%, fine grained, irregular fractures	Pl, (Ol)	
MS61-113	Dark grey, plagioclase 10% d=10mm, olivine <1% d=1-2mm, porous 8%, small grained, irregular fractures	Pl, (Ol)	